1966

Sintering study in the partially vitreous As-S-Se system

Michael Andrew Carrell
Iowa State University

SINTERING STUDY IN THE PARTIALLY VITREOUS As-S-Se SYSTEM

by

Michael Andrew Carrell

A Dissertation Submitted to the

Graduate Faculty in Partial Fulfillment of

The Requirements for the Degree of

DOCTOR OF PHILOSOPHY

Major Subject: Ceramic Engineering

Approved:

Signature was redacted for privacy.

In Charge of Major Work

Signature was redacted for privacy.

Head of Major Department

Signature was redacted for privacy.

Dean of Graduate College

Iowa State University
Of Science and Technology
Ames, Iowa

1966

TABLE OF CONTENTS

TABLE OF CONTENTS (Continued)

INTRODUCTION TO SINTERING

Vitreous materials comprise an important segment of engineering materials. The coalescence of vitreous materials by a flow process involves viscous and in some instances viscoelastic properties. These properties contribute to a flow transport mechanism imposed by the action of stress.

The expression sintering is usually applied to one or more of those complex processes involved in the densification of assemblies of particles at some temperature below the normal melting point of the material. The sintering process is fundamentally a phenomenon deriving from the thermodynamic requirement for an equilibrium system to seek a minimum of free energy. There is general agreement that the driving force for sintering, not considering externally applied stress, is due to the energy associated with large surface areas (1-3).

So far the terms melting point and equilibrium system have been used in the definition of sintering. The word vitreous implies neither a distinct melting point nor an equilibrium system; however due to the wide use of the word sintering, it shall be used in this thesis to describe the coalescence of vitreous materials.

The process of sintering must involve some initial surface interaction of atoms with the subsequent transfer of material into this region by one or more of a variety of possible mechanisms. It would appear to be helpful to list the elementary processes and factors which may lead to sintering, without saying anything at this stage about their importance in relation to or their various effect on the sintering mechanisms involved in this particular study. Thummler (4) does this satisfactorily.

Elementary processes

without transport of material	adhesion
with transport of material (atom movements over long distances)	
surface diffusion	movement of individual crystal-lattice components
lattice diffusion via vacancies	
lattice diffusion via interstices	
grain-boundary diffusion	
evaporation-condensation	
plastic flow	movement of whole regions of the lattice
viscous (and quasi-viscous flow)	
with transport of material (atom movements over short distances only--of the order of atomic distances)	
recovery or recrystallization	

Primary factors

- total contact surface
- crystal orientation
- diffusion coefficients
- surface tension
- viscosity coefficient
- critical shear stress
- vapor pressures and vaporization rate
- crystal structure and bonding state

Secondary factors

- surface activity (true surface structure)
- lattice activity (cold working, tensile and compressive stresses, lattice defects introduced during production, subdivision of secondary particles into primary particles)
- nascent states and allotropic changes
- foreign constituents
  - soluble
  - insoluble
  - surface films (e.g., oxide skins, soluble or insoluble during sintering, reducible or nonreducible, dissociable or nondissociable)
- gases (absorbed, occluded, and dissolved)

The kinetics of these different mechanisms in the sintering processes have been the subject of much study, and a complete review of the development of the current understanding of these processes is not practical. The subject has been thoroughly reviewed by several authors (1-10), and several bibliographies on sintering are available (11-15).

LITERATURE REVIEW

Viscous Flow

The mechanism of viscous flow occurs due to the stretching vibrations of bridging covalent bonds. When a structural unit overcomes a certain potential barrier it can be displaced in the process of flow. The free energy levels before and after the transformation are identical since the only process which has taken place is an activated change in the position of the atoms in space. The assumption here is that the transformation is not toward a more ordered arrangement which would involve a decrease in the free energy of the network.

To get somewhat of a structural insight into the complex process of viscous flow in glasses Nemilov (16) analyzed the change in the activation parameters over wide temperature and compositional ranges. A comparison of the values of the entropy of activation of viscous flow for different glasses in their softening range reveals knowledge of the structure of the glasses (16,17). Glasses formed by tetrahedrally bound structural units have the most extensive networks and therefore correspondingly low values for their entropies of activation (10-40 cal/mole·deg). Glasses in which the number of bridging bonds of the basic structural unit is equal to

three have much higher values for their entropies of activation (70-140 cal/mole·deg). Glasses formed by interweaving chain motifs have entropies of activation of approximately 300-500 cal/mole·deg.

Viscous Flow Sintering

The concept of viscous sintering was first developed by Frenkel (18) who derived an expression for the rate of coalescence of adjacent spheres under the action of surface tension. Using geometrical approximations for the purpose of studying initial sintering the Frenkel expression takes the form

$$\pi R_n^2 = \frac{3R_i \gamma t}{2\eta} \tag{1}$$

or at constant temperature

$$R_n^2 = kt \tag{2}$$

where R_n is the radius of contact between the two sintering spheres, R_i is the radius of an initial sphere, γ is the surface tension, t is the elapsed time, η is the viscosity, and k is a constant.

Equations explaining the sintering of vitreous materials have been based on the well known equation for Newtonian flow

$$\sigma = \eta \frac{de}{dt} \tag{3}$$

where σ is the acting shearing stress, η is the viscosity

of the material and de/dt is the strain rate. A number of authors (2,19,20) set the stress, σ, proportional to $-\gamma/\rho$ where γ is the surface energy per unit area and ρ the radius of curvature of the contact area between the two sintering spheres. Kuczynski (19) takes the quantity $dR_n/R_n dt$ as proportional to the strain rate, and for the initial stages of sintering he makes the geometrical approximation equating ρ to $R_n^2/2R_i$. Substitution of these quantities into Equation 3 followed by integration yields the Frenkel expression of Equation 2.

Sphere-sphere sintering data has consistently been published in terms of

$$R_n^x = kt \qquad (4)$$

where x is a constant for a particular compound or element. This equation is by no means antiquated. It has been used to describe very recent sintering studies of nonvitreous materials (21-23). The value for x has been experimentally determined to be two for sodium silicate glass (7,20,24). This value is used in the literature to describe the viscous flow mechanism.

With x equal to two, as in Equation 2, a constant contact area rate of growth would occur. No effort has been made to relate the sintering process to the surface area for

the sintering of viscous materials.

Kingery and Berg (7) and Kubo (20) have reported that linear shrinkage for the sintering of spherical glass particles (sodium silicate glass) follow the relationship

$$(\Delta L/L)^{5/2} = kt \qquad (5)$$

where L is the distance between the centers of the two initial spheres, ΔL is the shrinkage, k is a constant which depends on temperature, and t is the elapsed time.

Mackenzie and Shuttleworth (25) arrive at a theoretical format which expresses rate of sintering related to a material transport mechanism such as viscous flow. This flow alters the density by contracting holes within the material. This theory is said to describe fairly closely the latter stages of sintering. The volume contraction for sintering viscous bodies is represented by Clark and White (26,27). They started from the Kuczynski model and assumed that concave lens type layers were formed between particles. They further assumed that material from the surface other than at the contact zone flowed into this lens to cause volume contraction, and expressed this contraction as a function of time. This very complicated relation includes several empirical as well as assumed constants.

The amount of free energy available for the sintering of two vitreous spheres is rather small, consequently for sintering to take place the viscosity must be relatively low. For the sintering of sodium silicate glass spheres Kuczynski (24) calculated that at the temperature range of his experiments, the viscosity varied from 10^{10} to 10^{7} poises.

Viscosity

Viscosity is a property used to describe a viscous flow process. The magnitude of the viscosity depends upon the intermolecular forces, which in turn are determined by molecular size, shape, polarity, and other physical features. Inorganic vitreous compounds have the properties of covalent bonding and low coordination which generate a high viscosity when they are cooled from the melt state. As the temperature is decreased more interlinkage is obtained, and the resulting increased molecular weight gives a higher viscosity; indeed, viscosity measurements provide an important technique for determining molecular weights (28).

Viscosity is strongly temperature dependent. Glass at room temperature is a rigid solid possessing elastic and other characteristics of solid materials. At high temperatures where it can be characterized as a liquid, glass

possesses true viscosity and other characteristic properties of liquids. In an intermediate temperature range glass possesses the characteristics of both a liquid and a solid. This intermediate range is therefore often referred to as the viscoelastic range of glass.

We know that below the elastic limit of a solid Hooke's law can be considered valid, so that the average stress is proportional to the average strain where the proportionality constant is Young's modulus. A similarity exists between this relationship and Equation 3 where the rate of strain is proportional to the shearing stress. Here the proportionality constant is the coefficient of viscosity. The essential distinction between elasticity and viscosity is that the first is reversible and the second is irreversible.

When we consider polymers in the viscosity range beyond 10^8 poises (29), we must consider the viscoelastic ramifications. The viscous flow is restrained. In effect the viscous flow is retarded by virtue of the structural characteristics that include chain entanglement, cross-linking, and crystallinity.

By constructing models depicting the viscous and elastic attributes (29), it is possible to develop workable concepts

of the corresponding retardation time. The time rate of retarded strain occurring in a simple single spring and dashpot system (30) can be described uniquely by the retardation period τ. This parameter governs the exponential variation of strain ϵ with time t.

$$\epsilon = \epsilon_{\infty} (1-\exp[-t/\tau]) \qquad (6)$$

It has been suggested by Lontz (29) that for viscoelastic sintering the time-dependent interfacial coalescence could be more properly described using a correction to the Frenkel model

$$R_n^2 = \frac{3\gamma t}{2\pi\eta(1-\exp[-t/\Upsilon])} \qquad (7)$$

where η represents initial viscosity of order 10^8 poises and Υ an apparent relaxation constant to be assigned from experimental determinations.

Vitreous State

Some materials possess a high viscosity in the temperature region where their liquid would be in equilibrium with their crystalline states. This high viscosity enables the liquid material to cool at a relatively slow rate without maintaining equilibrium in the melt. The viscosity changes continually as we reduce the temperature to form a very highly viscous material. This nonequilibrium system therefore

"solidifies" in a noncrystalline state; i.e., the vitreous or glassy state.

A description of "the structure of the vitreous state" would indeed be most difficult. There are many prevalent ideas on the subject of vitreous structure, all the way from a complete random network to a simple assembly of molecules or other structural units. Most authors (31-35) agree that vitreous silica is a good example of a complete random network. Addition of alkali or alkaline earths to this vitreous silica could produce a severely broken down network or possibly regions of network with regions of broken down structure. It has been shown (36) that certain phosphate glasses contain quite long chains. In other words, the big controversy at the present time is <u>not</u> whether there is only one way of describing glass structure, but rather how much of each of the possible structures is present in different glasses.

A complete review of the development of the current understanding of this controversy is not practical. Mackenzie (37) and Frechette (38) have given such a discussion.

A few important points will however now be brought out regarding the categories of vitreous compounds in order to partially explain how a high viscosity, indicating strong

molecular interaction, can be reached without crystallization. Three common classes of vitreous compounds have been described by Prins (39) to be: oxide glasses like SiO_2 and B_2O_3; linear polymers like rubber and selenium; and smaller organic molecules, like glycerol, that are rich in OH groups. Zachariasen (40) explains the vitrification in the oxide glasses from the directional character and strength of the valency bond which form molecular connections in the melt. These configurations are difficult to readjust upon cooling. The linear polymers like rubber and selenium become entangled in the melt stage and upon cooling there exists the difficulty of disentanglement and reorganization for crystallization. Organic compounds like glucose glass have hydrogen bonds between molecules which keep crystallization from occurring (39).

If we look at inorganic vitreous compounds, in general we notice two striking similarities. They will have low coordination, and they will have covalent bonding. This can be put another way; the covalent bonding can provide low coordination together with the ability to form tightly held geometric configurations in two, three or four directions. In other words, vitrification is related to the chemical nature of the atoms and the electronic interaction between

them as well as thermal history.

Sulfur and Selenium Glasses

Chemically, sulfur and selenium are the most simple glasses known. Sulfur, depending on its modification melts at 112.8 or 115.2°C to a liquid of relatively low viscosity consisting of almost exclusively S_8 rings (41). Between its melting point and 160°C its viscosity is that normally expected from a nonassociated liquid; at 160°C the viscosity rises sharply due to the appearance of long chain material; and above 180°C it begins a gradual descent, which is caused mainly by the decrease in the number average chain length of the polymer (41,42).

There exists an inherent similarity in the behavior of selenium to that of sulfur with respect to the existence of linear chain polymers in the liquid state (42,43) as shown by the high viscosity of both liquids and the relative position of the two elements in the periodic table. However, in contrast to crystalline sulfur, hexagonal (metallic) selenium has been shown to consist of linear, long chain material (44), so that it is not surprising for polymer to appear at its melting point, 217°C. However, the other selenium modifications which consist of Se_8 rings, also seem to yield polymeric

material upon melting, so that in contrast to sulfur, no liquid region exists in which selenium is present exclusively as Se_8 rings (41). The viscosity of sulfur is an order of magnitude greater than that of selenium in the temperature range 218-327°C, and the number-average degree of polymerization in sulfur, to a first approximation, should be between one and two orders of magnitude above that of selenium (41). When sulfur and selenium are heated together, a copolymer is formed which is in equilibrium with S_8 monomer and Se_8 monomer (45).

As-S-Se Glasses

It is presumed that when arsenic is introduced into the S-Se system that it enters the polymers as a branch point giving rise eventually to a network formation. Vitreous materials in the S-Se binary system have been known for some time, but are known to devitrify readily when held at temperatures through which they were initially quenched. The addition of even small amounts of arsenic vastly decreases this tendency to devitrify with stable glasses resulting (46). This seems very consistent with the fact that arsenic, being of group V, can form three covalent bonds with sulfur and/or selenium.

Vaipolin (47) has found through the x-ray study of arsenic sulfide and arsenic selenide glasses that the bonds in these glasses must be predominantly covalent since the atomic spacings are closer to the sums of covalent radii than to the sums of ion radii. It is not unexpected, then, that stable glasses do occur in the As-S-Se system since covalent bonding and low coordination are both present. It would also seem quite probable that the extent of the As-S-Se vitreous system would be limited by the requirement that As-As bonds would not promote the vitreous state. A diagram such as Figure 1 would be expected. The experimental ternary by Flaschen (46) is given in Figure 2.

In crystalline arsenic sulfide, As_2S_3, chains of alternating arsenic and sulfur are bridged by sulfur to form a two dimensional net with each arsenic at the apex of a shallow triangular pyramid (48). In this net the alternating arsenic and sulfur atoms are arranged in nonplaner 12-member rings, forming two dimensional sheets (49). The glassy state of As_2S_3 has been experimentally studied using x-ray radial distribution analysis by a number of workers (47-52). If one assumes that the ring structure of crystalline As_2S_3 is present in the glassy state, the rings must adapt a wide

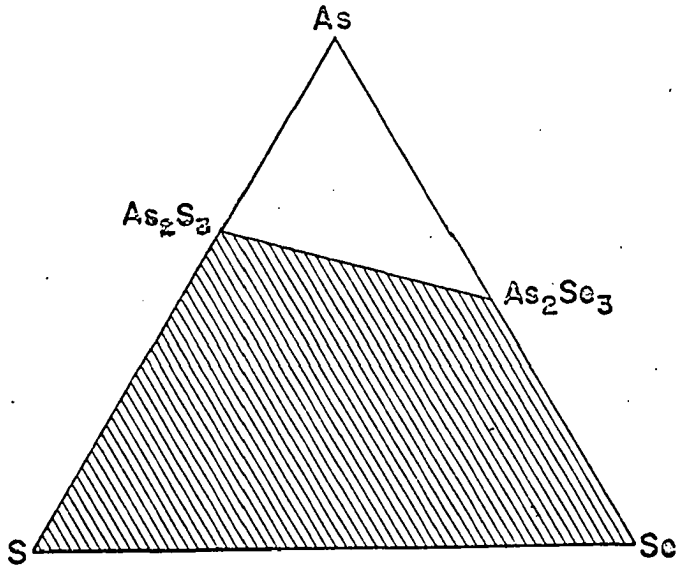

Figure 1. Weight per cent diagram of the As-S-Se system showing the expected vitreous region

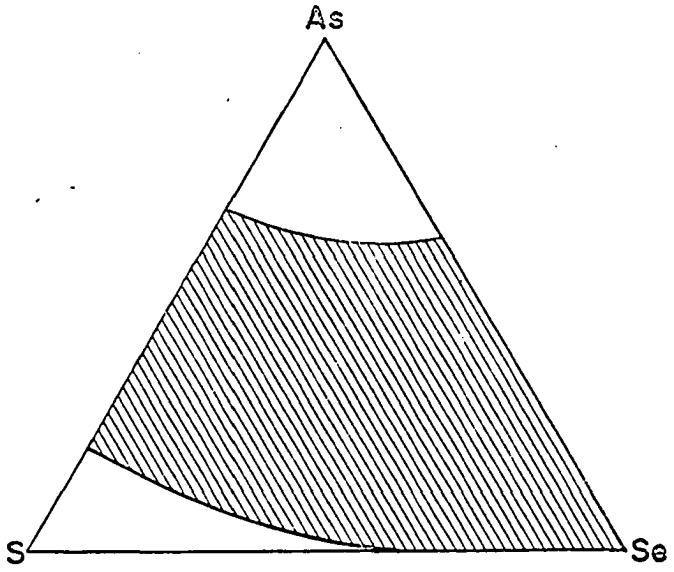

Figure 2. Weight per cent diagram of the As-S-Se system showing the extent of the vitreous region (Graph from Flaschen (46))

range of conformations. Hopkins and coworkers (49) report that such disorder is in accord with their x-ray findings. They noted that an important feature of the structure of crystalline As_2S_3 is a vector of 4.22 Å between atoms in a ring representing one of the repeat distances in the crystalline lattice. In glass such discord is in accord with the absence of a maximum of 4.22 Å in the radial distribution and with a very small density variation at values above 5 Å (49). A weak maximum at 4.22 Å was present in the data reported by Petz and coworkers (48). Apparently their sample retained an additional vestige of crystalline-like order that was not present in Hopkins' material.

There is general agreement on the bonding of arsenic to three sulfur atoms in vitreous As_2S_3 (47-53). The coordination of arsenic in vitreous As_2Se_3 is reported by Vaipolin and Porai-Koshits (54) to be greater than three. From their x-ray findings they have concluded that increasing the atomic number of an element of group VI of the periodic system to form a glass of the type $As_2(VI)_3$ increases the compactness of the symmetry of the glassy structure. They have proposed that the average coordination for arsenic in glassy As_2Se_3 is 3.5.

Experimental work done by Nemilov (55,56) on some As-Se glasses present a basis on which to describe the structure of As-Se-S glasses. In the region of compositions close to selenium (up to five atom per cent arsenic) the structure of the glasses is determined entirely by Se-Se linkages since the values of the entropies of activation of these compositions are close to the values of the entropy of activation of viscous flow for vitreous selenium (over 300 cal/mole·deg). In the region of five atom per cent arsenic to 17 atom per cent arsenic the entropies of activation are independent of the change in composition, and are 140 $\pm$ 10 cal/mole·deg--the average for the values characteristic for chain bonded glasses and/or for trivalently bonded skeletons. From approximately 20-40 atom per cent arsenic the entropy of activation has values of about 80 cal/mole·deg which indicates a complete spatial predominance of trigonally bonded structural units in glass.

INTRODUCTION TO PROJECT

An objective of this sintering project was to relate the decrease in surface area during sintering to the rate of sintering of vitreous substances. It was thought desirable to observe the above relationship for a number of internal glass structures. Spherical samples of these glass structures would provide an approach for determining measurements of area.

Certain difficulties were inherent: a constant temperature environment for the sintering experiments, direct observation of the sintering spheres at sintering temperatures, initial formation of spherical samples, and adhesion of the spheres to their supporting filament. To minimize these difficulties a system of glasses which exhibited low viscosities at relatively low temperatures was sought. Low melting phosphate and silicate systems were considered; however, these are known to be very hygroscopic due to the necessity of including high percentages of flux in their compositions, such as sodium or potassium oxides. The intermetallic systems involving group V and VI elements were considered since they form low melting vitreous systems.

Both sulfur and selenium can form elemental glasses

consisting of long chain units, and since they both form vitreous binary network systems with arsenic, the As-S-Se ternary system was chosen for this study. The conclusions drawn from the literature review of the As-S-Se vitreous state are significant. Many different types of internal glass structures exist in the As-S-Se ternary system. The density of packing and properties of the covalent bonds which determine the viscosity in this system vary distinctively with composition. This is in contrast to oxygen glasses which possess a constant short range order when their long range structure is "broken-down" by addition of modifier cations. Figure 3 shows the vitreous compositions chosen and studied in this project.

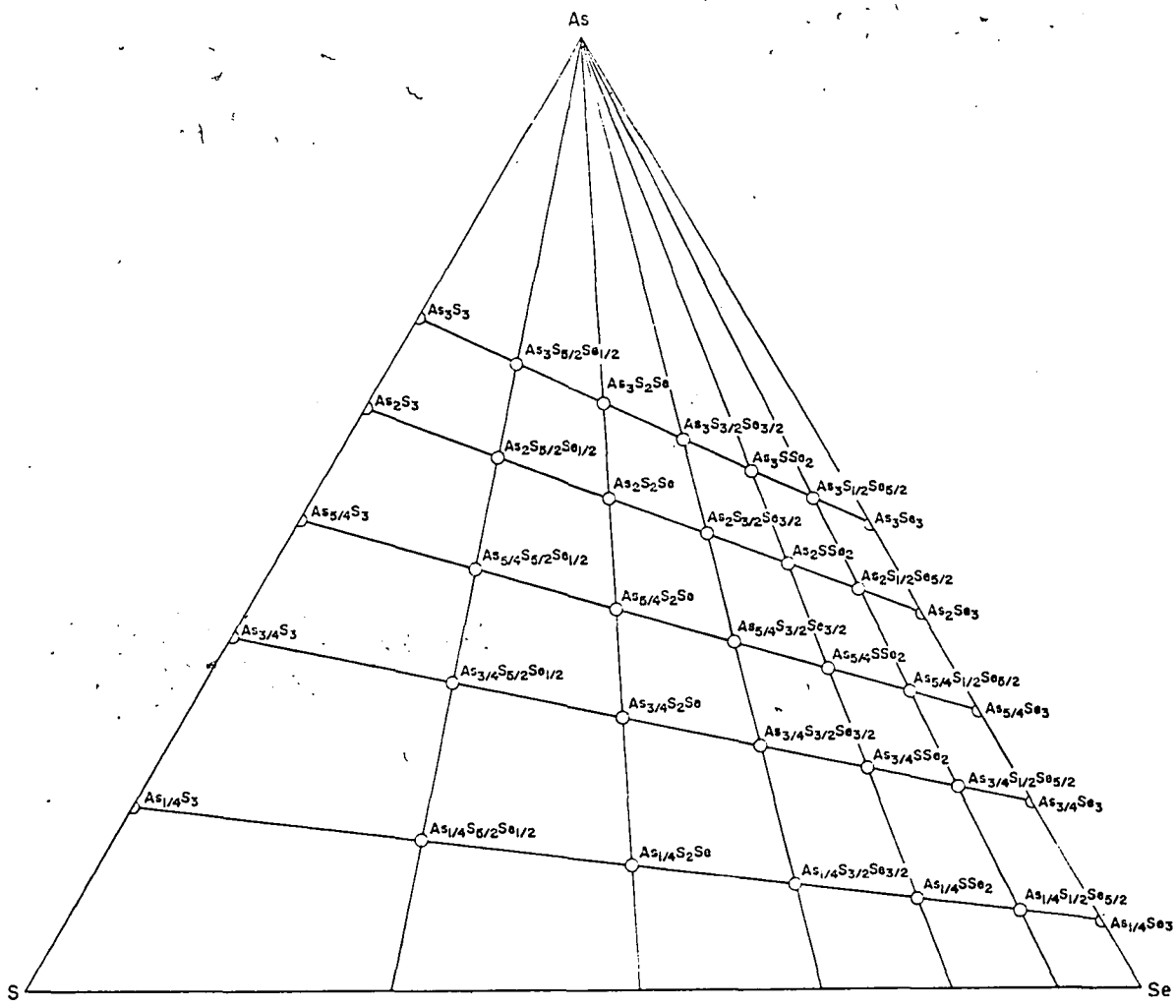

Figure 3. Weight per cent diagram of the As-S-Se system showing the vitreous compositions studied in this project

EXPERIMENT

Sample Preparation

Appropriate quantities of selenium (Fisher, certified), sulfur flowers (Baker and Adamson), and arsenic powder (Pennsylvania Rare Metals Incorporated, 99.99 purity) were weighed on a Mettler balance to the nearest 1/10,000 of a gram. The sample size for a glass composition varied between five and ten grams. After weighing the elemental powders, each was added through a funnel into a narrow mouth vycor ampoule. The sides of the funnel and ampoule were washed down with methyl alcohol after each addition, and the three elements were then wet mixed by agitation. The ampoules were then placed in a drying oven to evaporate the alcohol. After drying, the ampoules were evacuated, and then sealed in vacuo with an oxygen-gas torch.

The evacuated ampoules were then placed in a steel bomb inside of a silicon-carbide resistance furnace. The bomb could be rotated from outside of the furnace to promote homogeneity of the melt. A temperature of 525^{o}C was held for six hours with intermittent rotation of the steel bomb. The furnace was then opened, and the ampoules were removed and allowed to air quench at room temperature. Compositions,

except for those with very high sulfur content, would easily break away from the inside of the vycor ampoules on cooling because of the difference in coefficient of expansion of the two materials. An ampoule was wrapped in cloth and broken by striking the contained ampoule with a plastic mallet. An implosion would occur when the vycor was broken due to the outside air pressure. The material was unwrapped, and the As-S-Se composition was separated from the vycor. The material was placed in appropriately labeled bottles and placed in a desiccator for storage. Samples sent for wet chemical analysis verified the initially projected compositions.

Sphere Formation

Each glassy composition was crushed using a porcelain mortar and pestle. The high sulfur containing vitreous compositions were wet ground with alcohol to obtain a crushed powder. This was necessary since the high sulfur containing material would agglomerate during dry crushing.

Nearly perfect spheres of a variety of materials have been prepared by Kingery and Berg (7) using arc fusion. The material of desired particle size was fed into the center of a three-phase carbon arc through a graphite tube extending into a chamber surrounding the arc. A closed chamber was

used to decrease convection currents around the arc. Since a low-melting ternary was chosen for this project, it was thought that spherical samples could be obtained by passing the crushed material through the mouth of a small tube furnace. The material was allowed to fall through the hot zone of the tube furnace and then out of the bottom to be quenched by room temperature air traveling up through the tube. A beaker was placed below the tube to collect the spherical material.

A half-inch diameter, six inch long platinum wound tube furnace was used for this purpose. The furnace had a hot zone with a length of one inch which was located in the middle of the tube length. The furnace was supported in a vertical position on two refractory bricks, and a beaker was placed between the bricks to collect the falling material. A vycor funnel was placed above the furnace and extending into the mouth of the furnace through which the crushed material was added.

The furnace was located in a hood due to the volatilization of the compositions during sphere formation. Initially the furnace was placed in a dry box which was fed a positive pressure of nitrogen and vented to the hood. However since

the volatilization of these compositions was high, no physical or chemical difference could be found between spheres formed in the nitrogen atmosphere or in air. Spheres of all thirty-five compositions were therefore made in air because of the ease of this operation.

Two variables were considered in the formation of spheres--initial particle size of the crushed compositions and furnace temperature. A powerstat was used to control the furnace temperature. A thermocouple was placed at the middle of the hot zone through which the material would fall, and a temperature versus power input calibration was determined for the furnace. Crushed glassy As_2S_3 was used to determine what approximate particle size and what temperature should be used for sphere formation. Spheres as small as 90 microns were made at a number of furnace temperatures: 600, 655, 725, 775, and 850°C. The temperature range of 600-655°C produced the largest number of spheres. Spheres of 90 microns in diameter were the smallest that could be formed because of the reverse flow of air through the furnace. The higher the temperature the more vaporization of material occurred. It was found that when the initial particle size was below 200 mesh, the particles did not separate from each other as they were

dropped through the funnel into the furnace core. These agglomerates did not form spheres. It was found that a wide distribution of particle sizes separated from one another easily when dropped through the furnace. The efficiency of sphere formation varied with composition and temperature in this project. A temperature of from 600-700°C was used--optimum conditions gave 75-95 per cent conversion of crushed material to spherical particles.

The crushed materials were tapped from a small spatula into the funnel from which the material fell through the furnace. After a few milligrams were passed through the funnel, it was replaced with a clean funnel and the process repeated. This was necessary since the funnel became hot and the material would not slide down its sides readily. Rubber gloves were used as protection against the volatilized material.

The beaker containing the collected quenched material was washed with alcohol, and the spheres were separated by the rolling movement they possessed under agitation. The spheres were examined for number and uniformity to see if the furnace temperature would need to be changed i.e., if only a small number of spheres were present in the collection the process

would be repeated at a higher or lower temperature.

Spheres of each composition were embedded in resin, and their cross-sections were observed to be free of voids. X-ray analysis of the spheres showed that all thirty-five compositions were vitreous in nature. The spheres used in this project were considered uniform. A uniformity check was accomplished by measuring the diameter of a sphere in different positions using a filar inserted in the eyepiece of a Leitz petrographic microscope. Sphere diameters measured in this manner did not vary more than one per cent. Chemical analysis of the spherical material showed no apparent chemical difference from that of the initially crushed material.

(Low melting lead and phosphate glasses were crushed and fed to the furnace at higher temperatures than those used for the As-S-Se ternary. Vitreous spheres were easily obtained.)

Equipment

Figure 4 shows schematically the experimental arrangement used for the sintering experiments. In order to observe the coalescence of vitreous spheres a microstage furnace was used. The furnace consisted of simply an electrical heating filament supported by watercooled brass contacts. The watercooling was not used in this project since the sintering

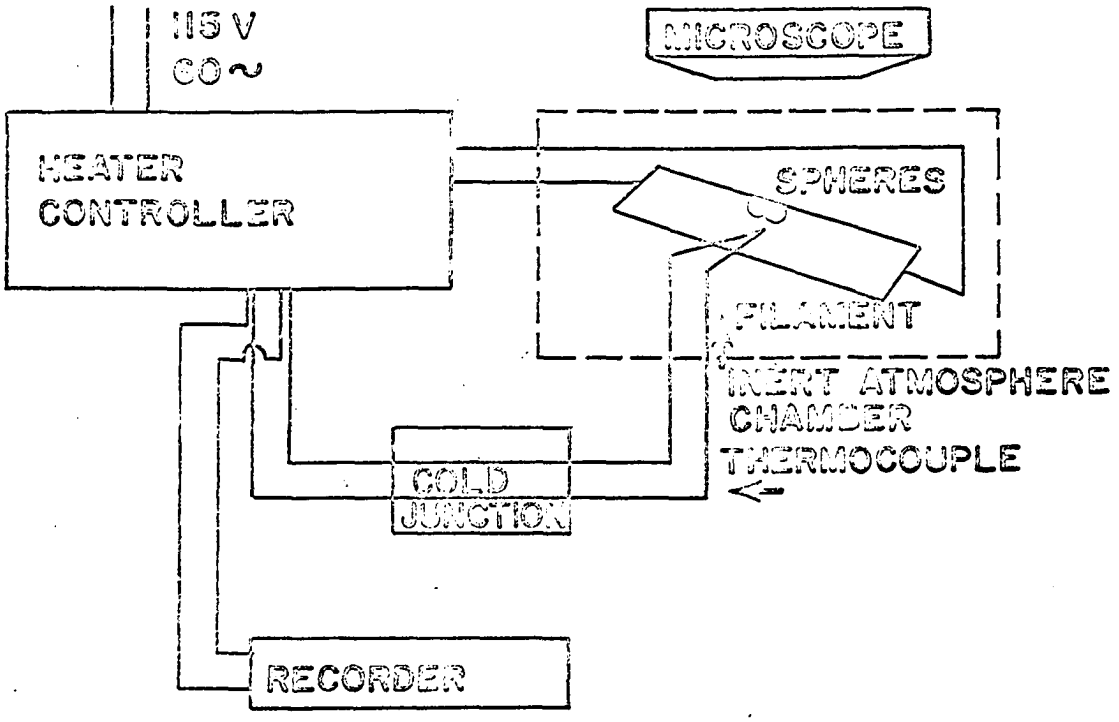

Figure 4. Arrangement used for the sintering experiments

temperatures were relatively low. The furnace was enclosed so the sintering could be done in a nonoxidizing atmosphere. The chamber was necessarily constructed with a plate glass window for observation.

The voltage was supplied from a 115 a.c. line. This input was regulated by a saturable reactor in the scheme shown in Appendix A.1. The temperature of the stainless steel filament was measured with a chromel-alumel thermocouple--its hot junction was spot welded to the filament. The hot junction was connected to a cold junction at $0^{o}C$ and fed to the balancing system referred to in Appendix A.1. and to a recorder. A temperature in the range of 50-350^{o}C could be maintained indefinitely using this apparatus to an accuracy of $\pm$ 1/8 C^{o}. A leitz petrographic microscope was mounted to focus on the heating filament through the plate glass viewing window. The microscope was used with a filar eyepiece for direct measurements.

Experimental Technique

Spheres of a given composition were washed out of a storage bottle onto a watch glass. The watch glass was placed under a microscope, and with a probe two spheres of similar size were chosen and separated from the rest. A filar was

used in conjunction with a microscope to pick two spheres of nearly identical size. The selection occurred from hundreds of spheres which had a narrow size distribution--caused by the method of production.

One of the fortunate results of picking a low melting ternary occurred in connection with the filament coating. A thin coating of high temperature vacuum grease (Apiezon, melting point approximately 250°C) was applied to the stainless steel filament to protect against sphere adhesion to the filament. Such a situation was necessary when measuring linear shrinkage of coalescence. The sintering experiments were done in a nonoxidizing atmosphere to assure that this grease would not oxidize.

The selected spheres were transported in a watch glass to the filament where a probe was used to place the spheres in contact on the filament. This was accomplished by using a coating of water on the probe the surface tension of which kept the two spheres together while they were transported to the filament. The spheres were released by gentle contact with the greased filament, and the spheres were kept in contact by the surface tension of the water. Care was taken to place the spheres in close proximity of the thermocouple;

i.e., one to two millimeters. At that distance from the thermocouple, which was placed in the middle of a five centimeter long filament of constant width and thickness, the temperature variation from that of the thermocouple was approximately ± one centigrade degree. This variation was estimated by holding the filament at a constant temperature and probing the filament with a thermocouple.

The glass viewing plate was placed above the filament, the microscope was adjusted, the filar was aligned for a sintering measurement, a partial vacuum was drawn on the chamber by a mechanical pump, and finally helium was allowed to flow into the chamber keeping only a slight negative pressure to hold the viewing plate in place. The nonoxidizing atmosphere was not only used to prevent sphere oxidation products from forming, but also to keep the filament lubricating grease from oxidizing.

It should be mentioned that at each composition a preliminary run was taken to establish the temperature range for the sintering experiments. The temperature was taken up at five degree intervals until the flow could be observed to form a neck growth within a matter of minutes. Then temperatures in this region were chosen for study for this particular composi-

tion.

With the power turned on, a chosen temperature was obtained by manually turning a dial to the necessary thermocouple output. This took a number of seconds, and the experimental elapsed time was not begun until the desired dial reading was reached (the filament temperature trailed the dial reading only momentarily). This procedure was followed to keep the temperature from momentarily overshooting the desired dial reading during the initial "hunt". Such an overshoot would occur if the dial was set to the desired thermocouple output before the power was turned on.

To take a reading the following procedure was followed. The filar was set on one edge of the sphere or neck diameter and the reading noted. While the time was being observed the filar was turned to the opposite edge. The first edge reading was written down along with the time, and then the last reading was taken from the filar. A two to three second lag occurred between measurements. This error was insignificant at relatively long sintering time periods.

To a close approximation 100 units on the filar equaled 100 microns. (A calibration was made at the magnification used showing that 100 units equalled 98 microns.) The

average sphere size used in the experiments was approximately 200 microns in diameter. A Leitz petrographic microscope was used; however since the limit of resolution is one to two microns, some error in measurements undoubtedly occurred.

SINTERING MODELS

Three models were postulated as possible geometric configurations which the sintering process might follow. These models were thought to represent both possible extremes in the sphere-sphere sintering process (initial radii increasing and initial radii decreasing) and an intermediate model where the initial sphere radii remain constant. It was thought that the sintering process would resemble one of these models, and then appropriate modifications would be made on this model to represent the sintering process. Surface area could then be related to the sintering rate of viscous materials.

The models were chosen with a restriction of constant volume: a) Neck growth would occur with the centers of the spheres coming closer together. Overlap of the spheres would go to increasing the radii of the spheres (Figure 5a and Appendix B.1.). b) Neck growth would occur with the centers of the spheres coming closer together. The sphere radii would remain constant, and the overlap of the spheres would go to form a cylinder between the spheres (Figure 5b and Appendix B.2.). c) Neck growth would occur without the overlap of spheres; however, the spheres would become smaller and the excess material would form a cylinder between the spheres

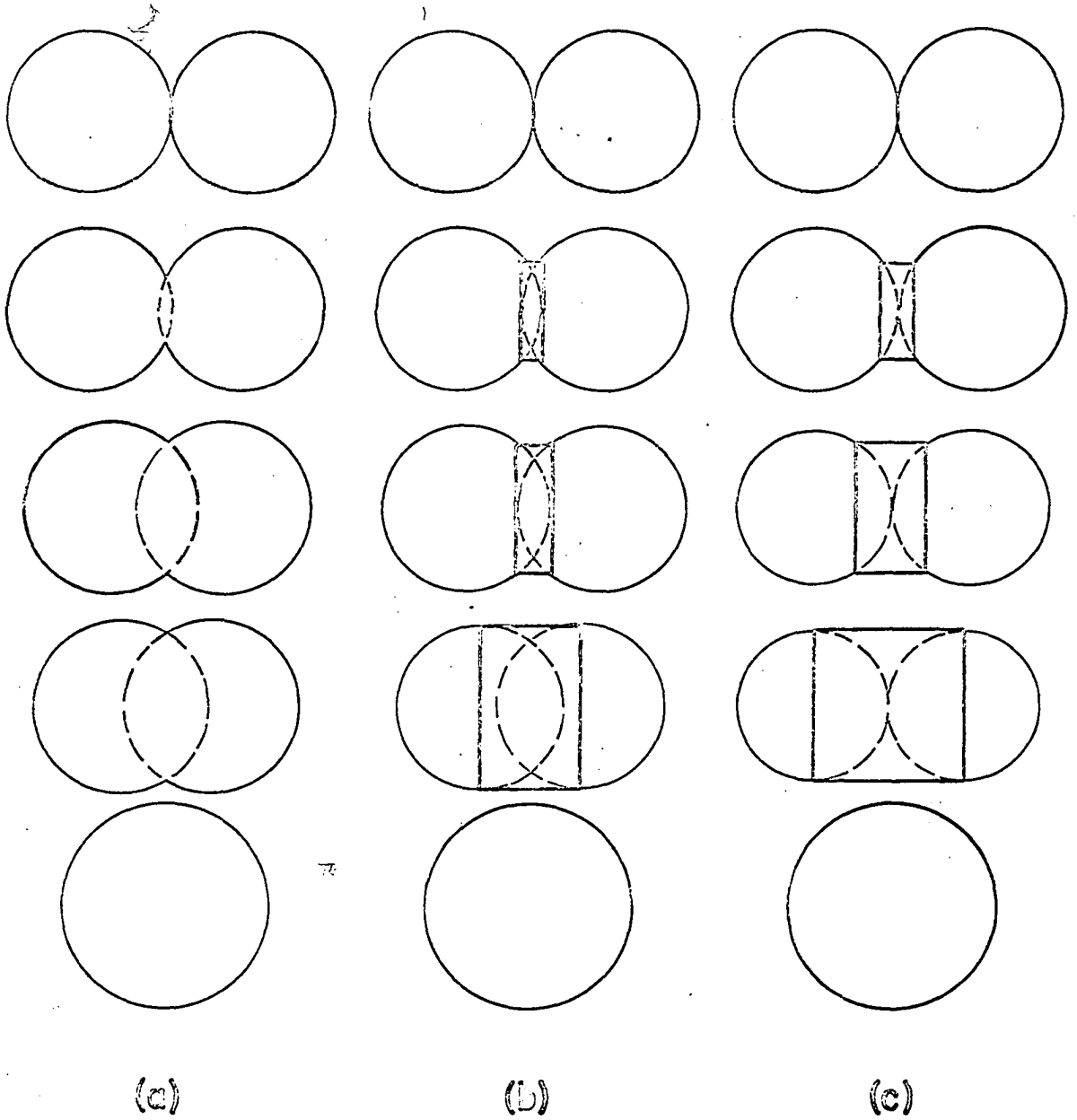

Figure 5. Sintering models
(a) radii increasing
(b) radii constant
(c) radii decreasing

(Figure 5c and Appendix B.3.).

R_n/R_i versus A/A_f for these three models are shown in Figure 6, where R_n is the neck radius, R_i is an initial sphere radius, A is the surface area, and A_f is the final surface area when one sphere of radius $2^{1/3}$ R_i has been formed. R_n/R_i versus L/L_i are shown in Figure 7, where L is the length of the two spheres during sintering and L_i is the initial length of the two spheres, $4R_i$. A/A_f versus L/L_i are shown in Figure 8.

It was found that when the sintering data were taken, the sintering sequence followed that shown in Figure 9. This particular sequence was for the composition $As_{5/4}S_{5/2}Se_{1/2}$. It can readily be seen that the initial radius does indeed remain nearly constant. Experimentally determined values of L/L_i versus R_n/R_i for a number of compositions were superimposed on Figure 7, and it can be seen that this experimental data followed the model of constant initial radii consistently and closely. (Since the experimental data produced two sets of data, R_n/R_i versus time and L/L_i versus time, R_n/R_i versus L/L_i were determined graphically.) It was therefore decided to use this surface area versus neck-radius relationship of constant initial radii,

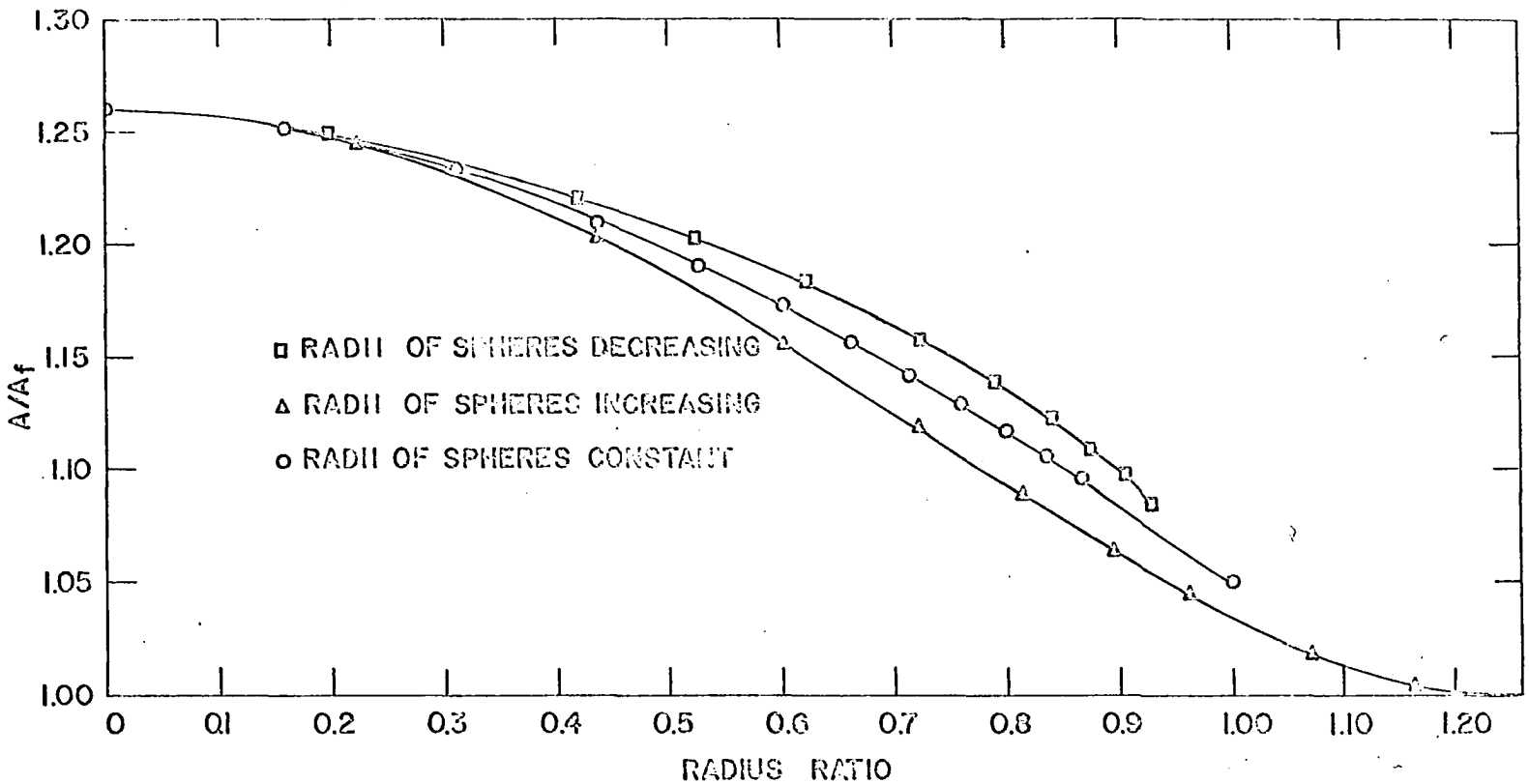

Figure 6. A/A_f versus radius ratio for the sintering models

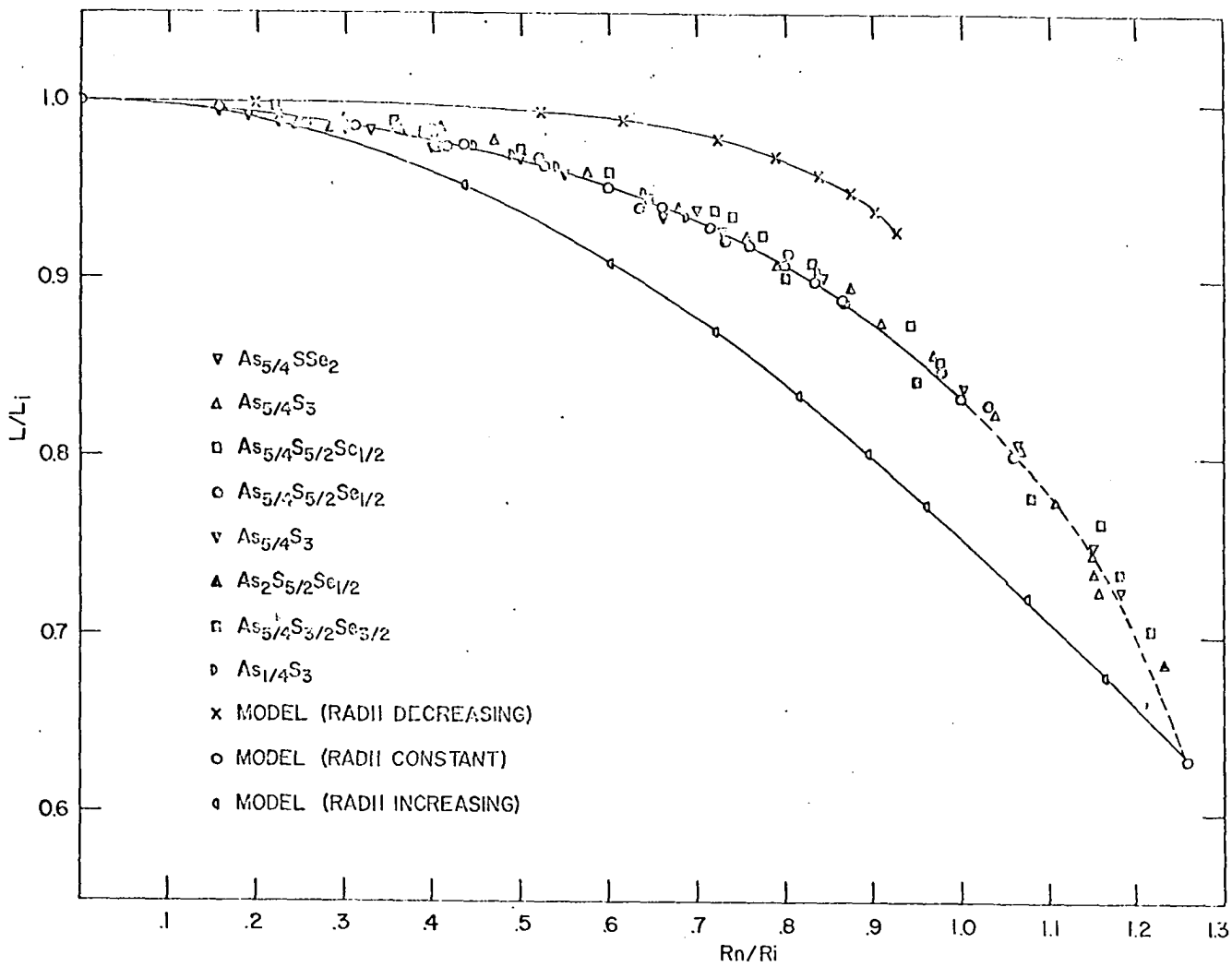

Figure 7. L/L_i versus R_n/R_i for the sintering models
Experimental sintering data is superimposed

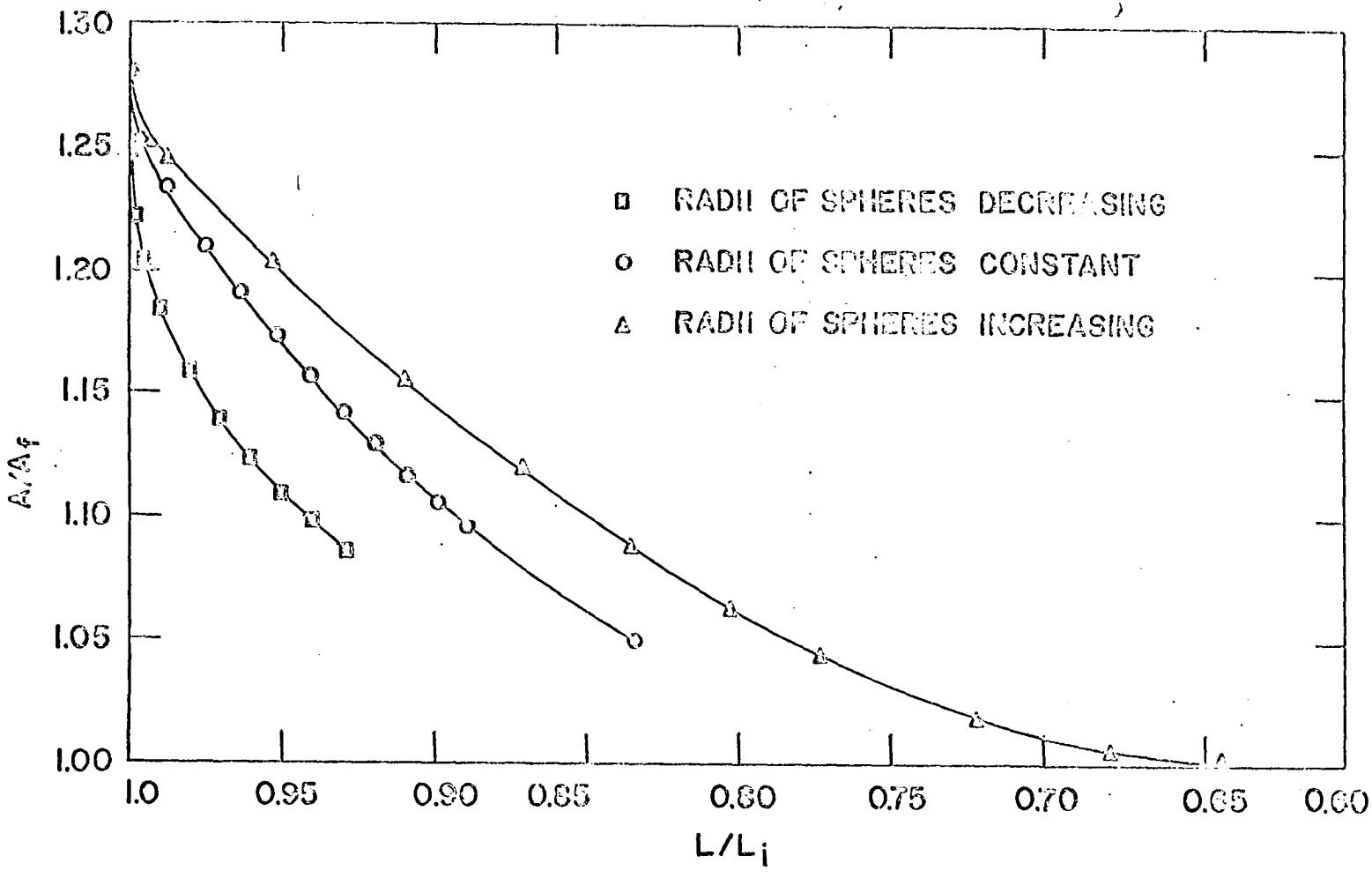

Figure 8. A/A_f versus L/L_i for the sintering models

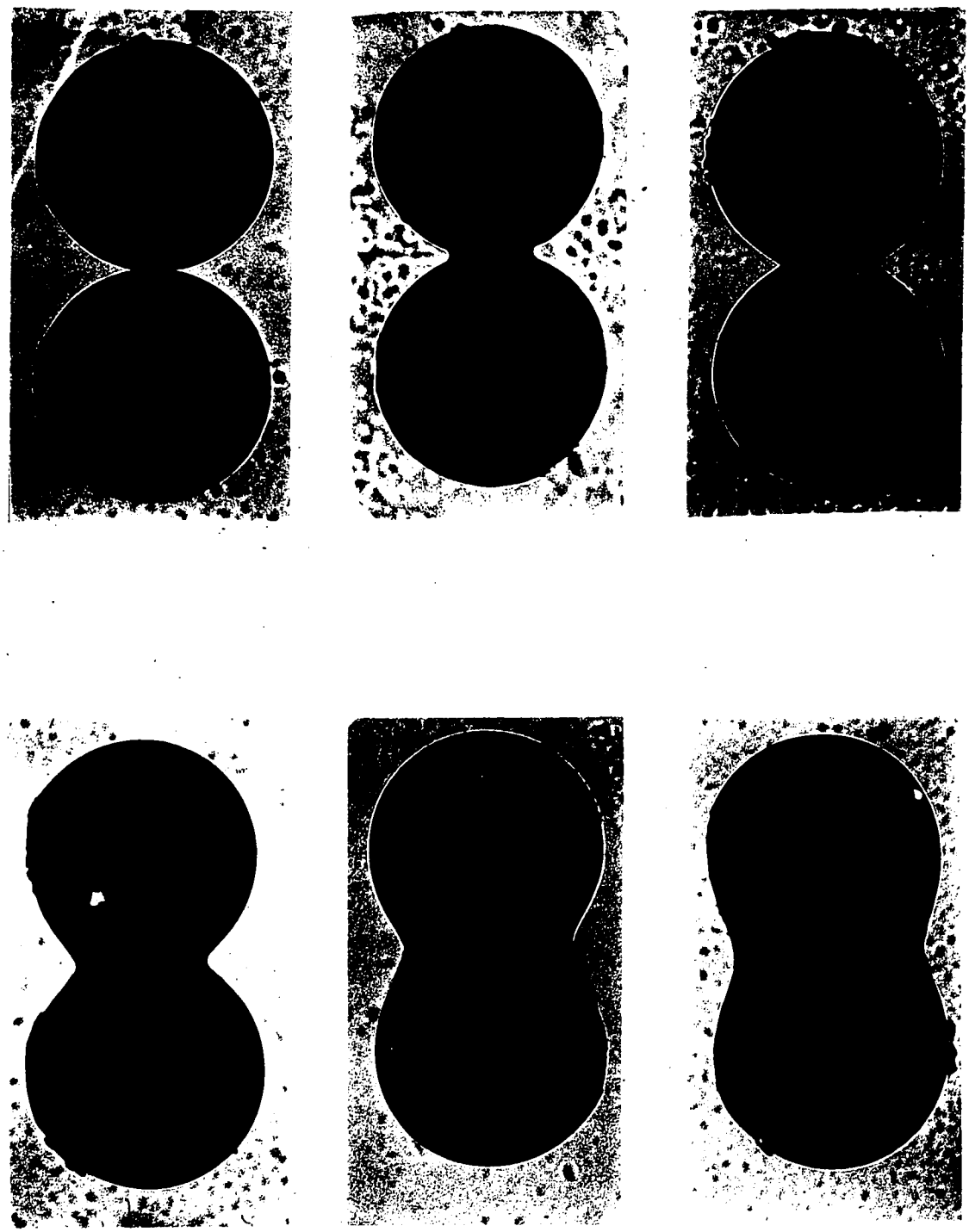

Figure 9. Sintering sequence for the composition $As_{5/4}S_{5/2}Se_{1/2}$

$$A/A_f = 1.26 - 0.01785(R_n/R_i) - 0.2419(R_n/R_i)^2 + 0.04987(R_n/R_i)^3 \qquad (8)$$

to relate the surface area to the sintering rate of viscous spheres. (Equation 8 was obtained by using a least square computer program for the best cubic fit.)

It should be noted that some deformation of the vitreous spheres during sintering did occur by the force of gravity; i.e., a flattening of the sphere in contact with the filament. Therefore the actual surface area was greater than that presented by the model. However, if one postulates that the neck formation would proceed similarly under conditions where the gravity force could be eliminated, the area versus neck-radius relationship for this model could be used. This postulate seems very plausible, and the area relationships will be expressed under this assumption.

RESULTS

Logarithm R_n/R_i Plotted Against Logarithm Time

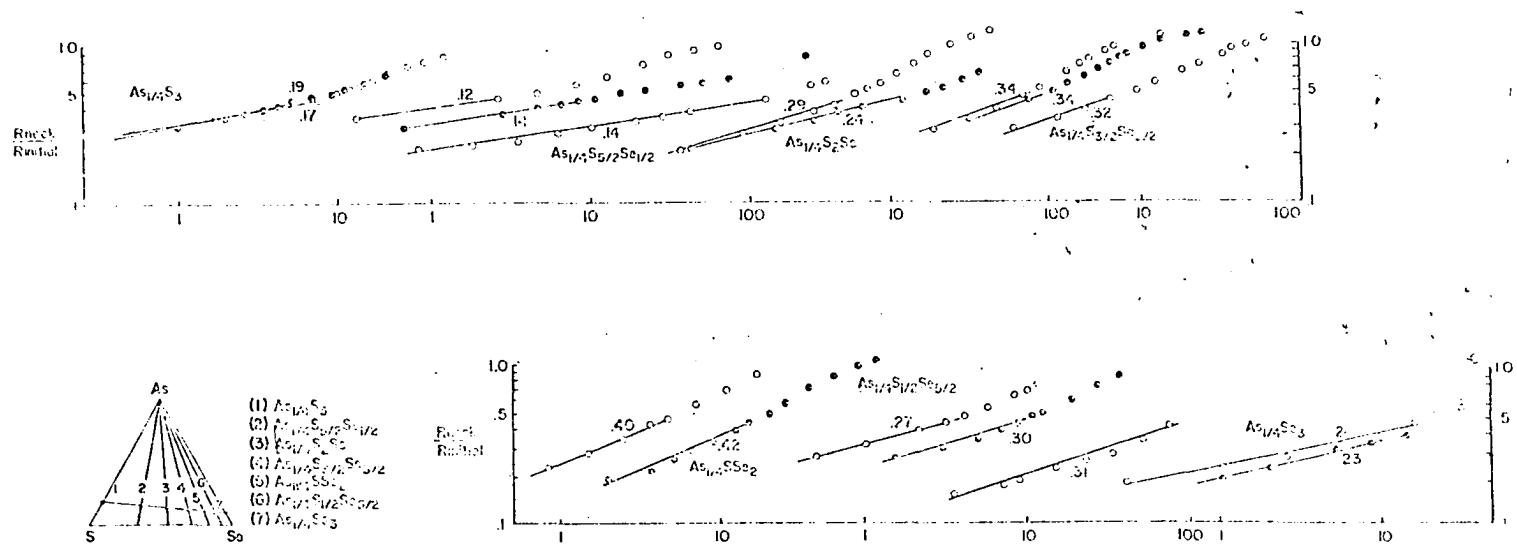

Figure 10. Logarithm R_n/R_i versus logarithm time for compositions $As_{1/4}(S,Se)_3$

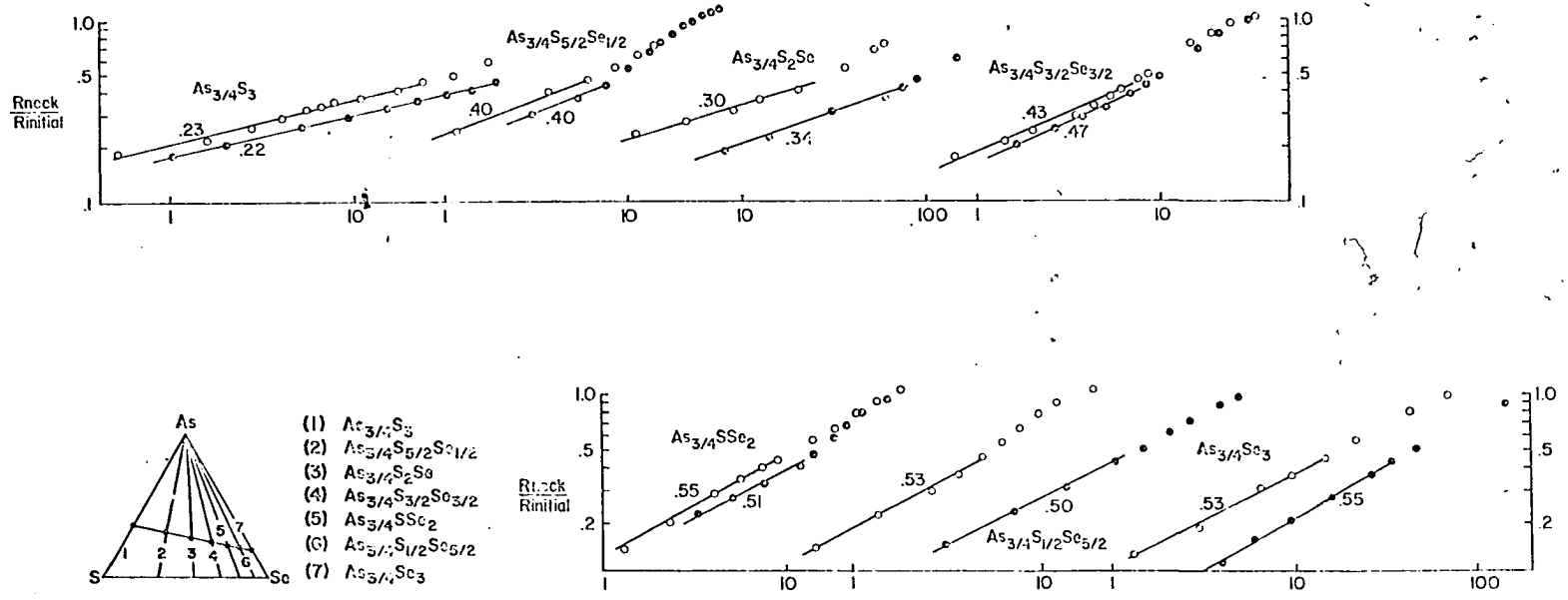

Figure 11. Logarithm R_n/R_i versus logarithm time for compositions $As_{3/4}(S,Se)_3$

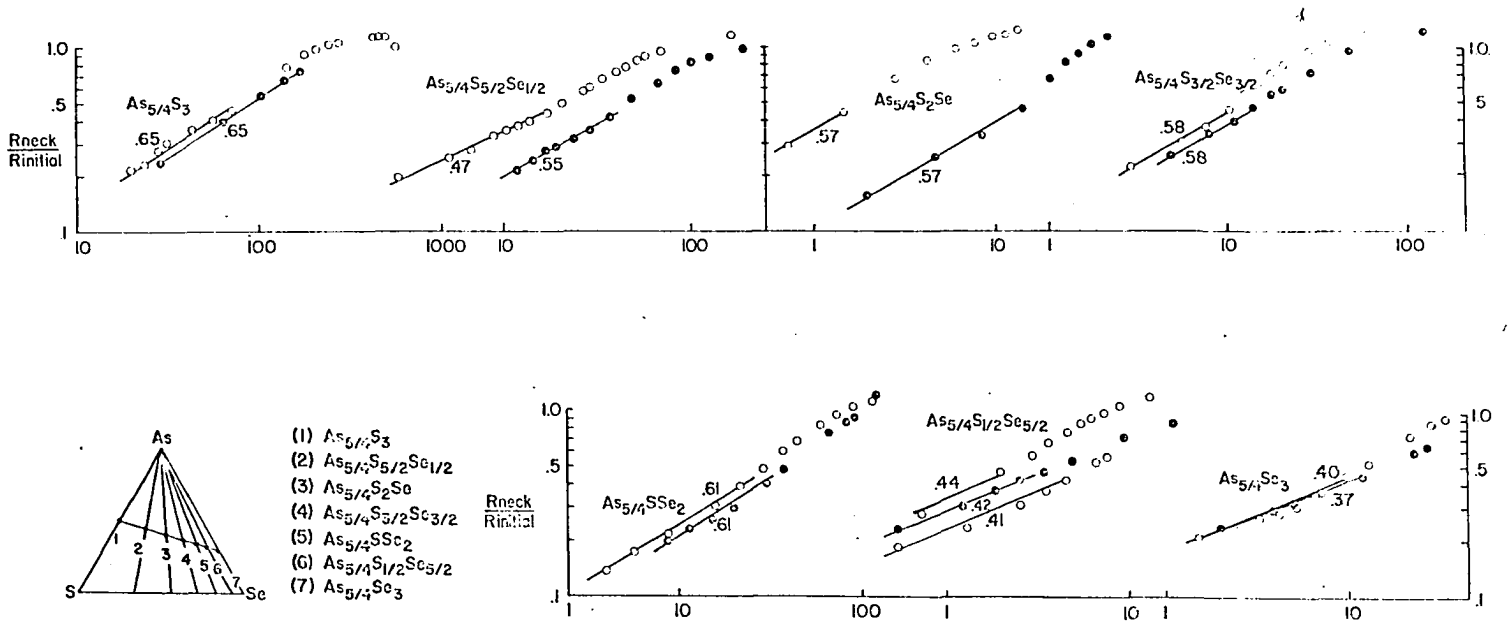

Figure 12. Logarithm R_n/R_i versus logarithm time for compositions $As_{5/4}(S,Se)_3$

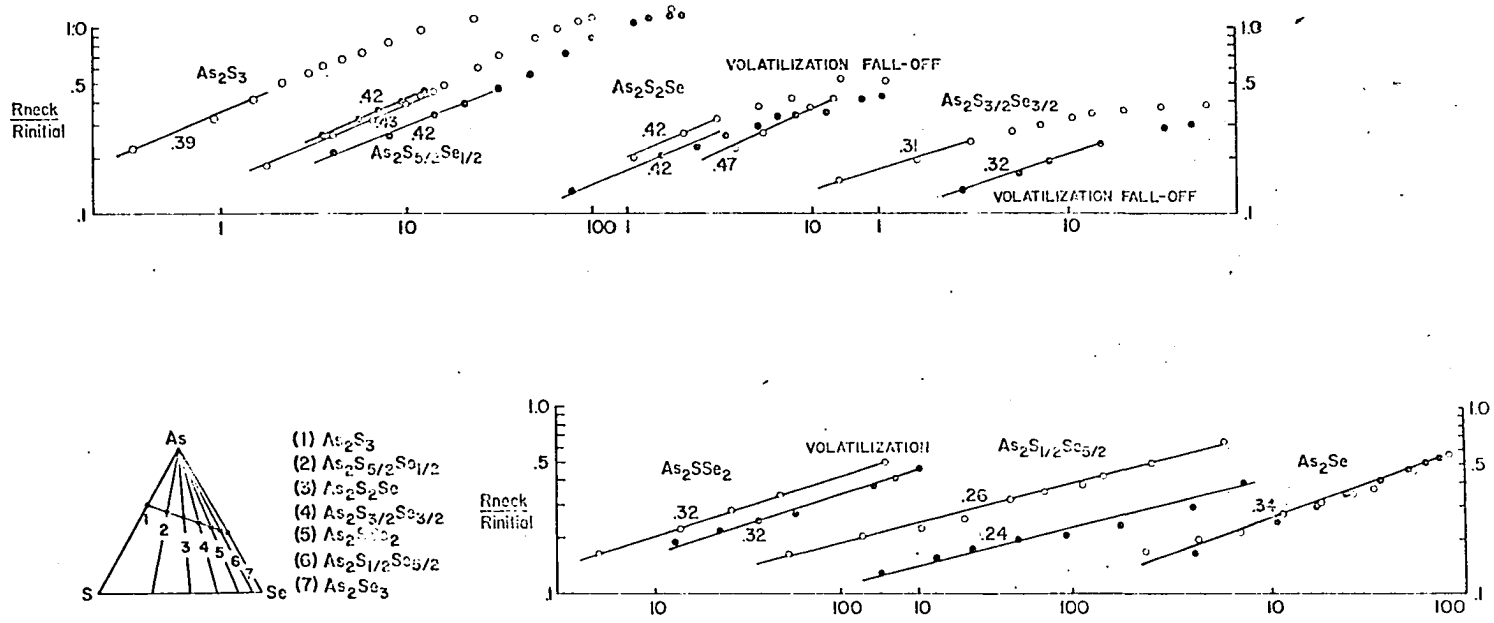

Figure 13. Logarithm R_n/R_i versus logarithm time for compositions $As_2(S,Se)_3$

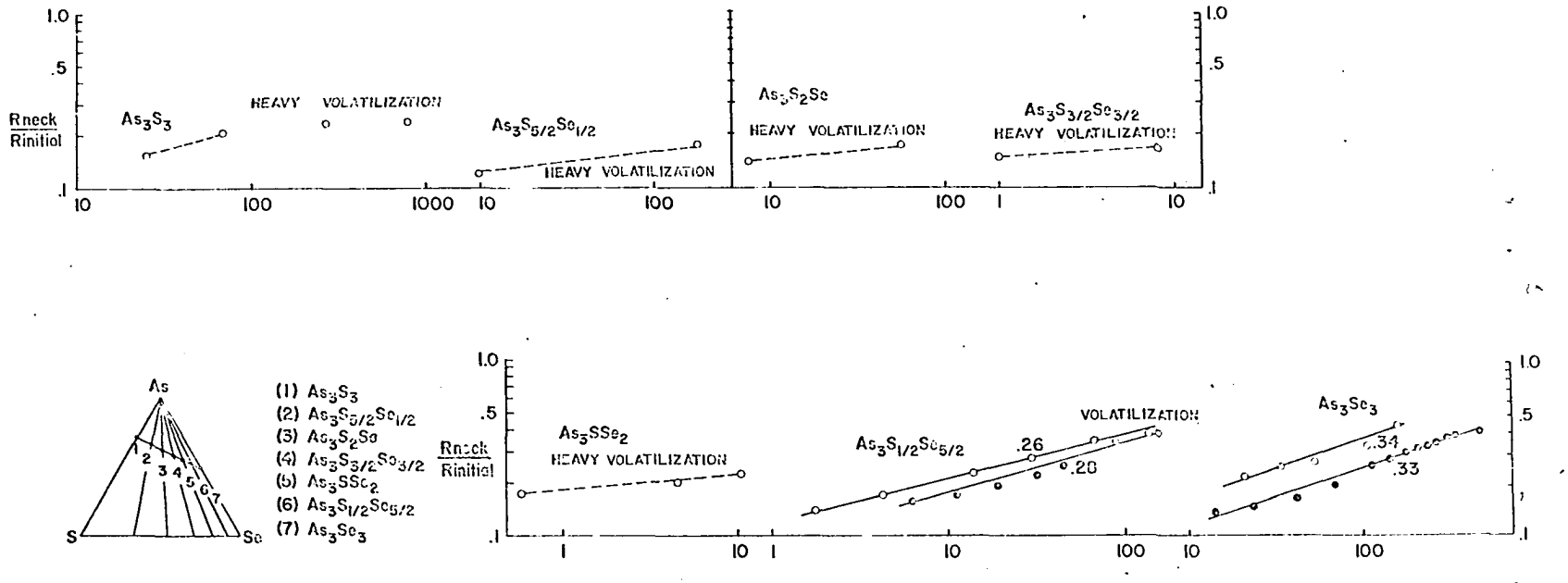

Figure 14. Logarithm R_n/R_i versus logarithm time for compositions $As_3(S,Se)_3$

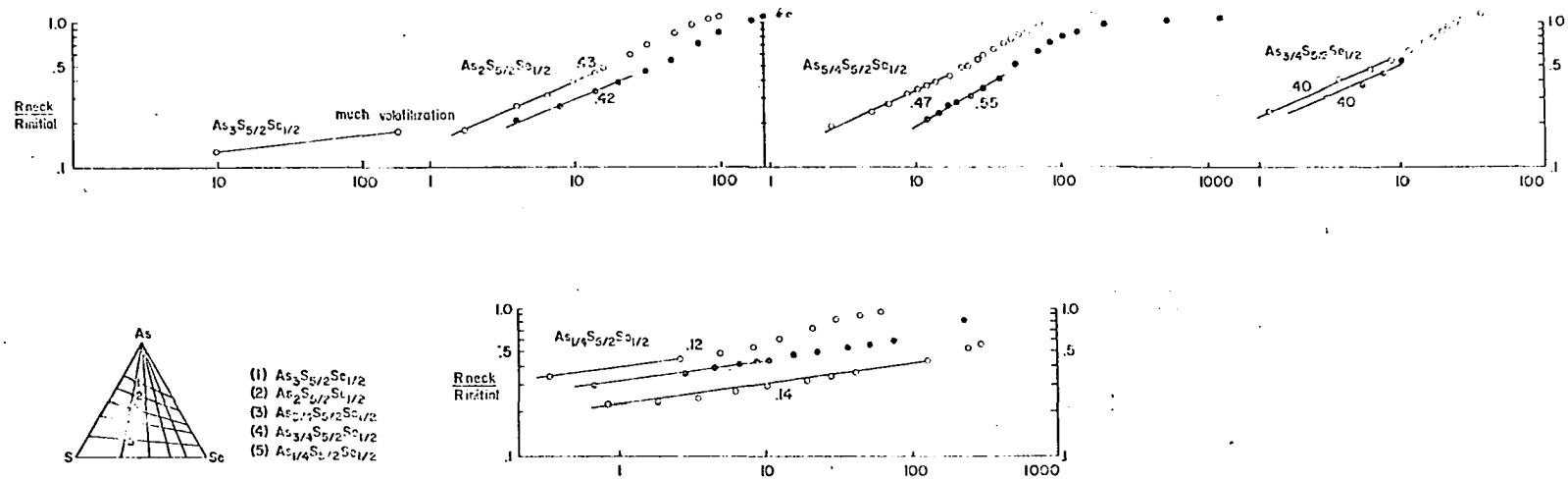

Figure 15. Logarithm R_n/R_i versus logarithm time for compositions $As_xS_{5/2}Se_{1/2}$ where x has values of 3, 2, 5/4, 3/4 and 1/4

A/A_f Plotted Against Time

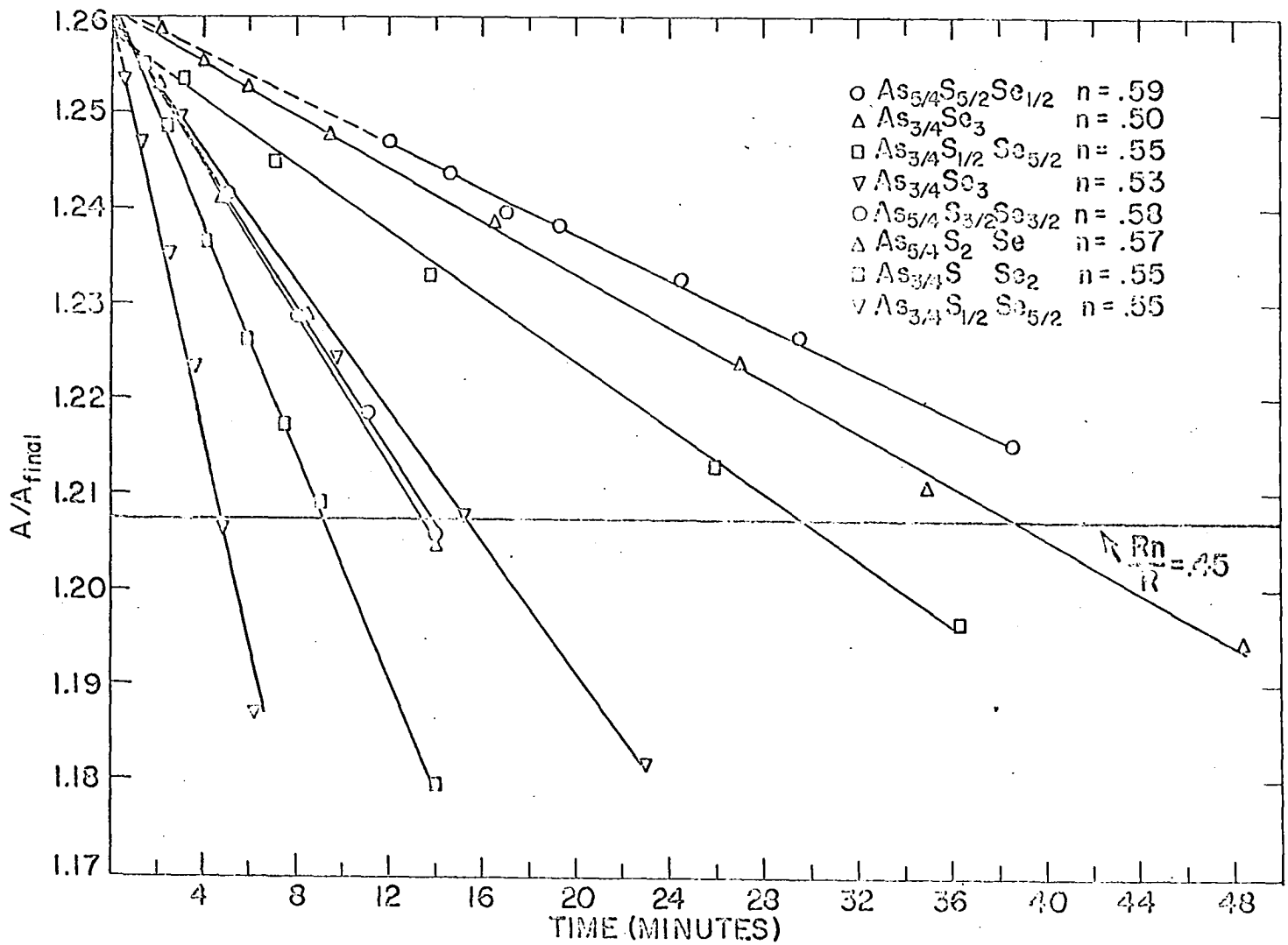

Figure 16. A/Af versus time for compositions with n-values greater than 0.5 where n is the slope of logarithm R_n/R_i plotted against logarithm time

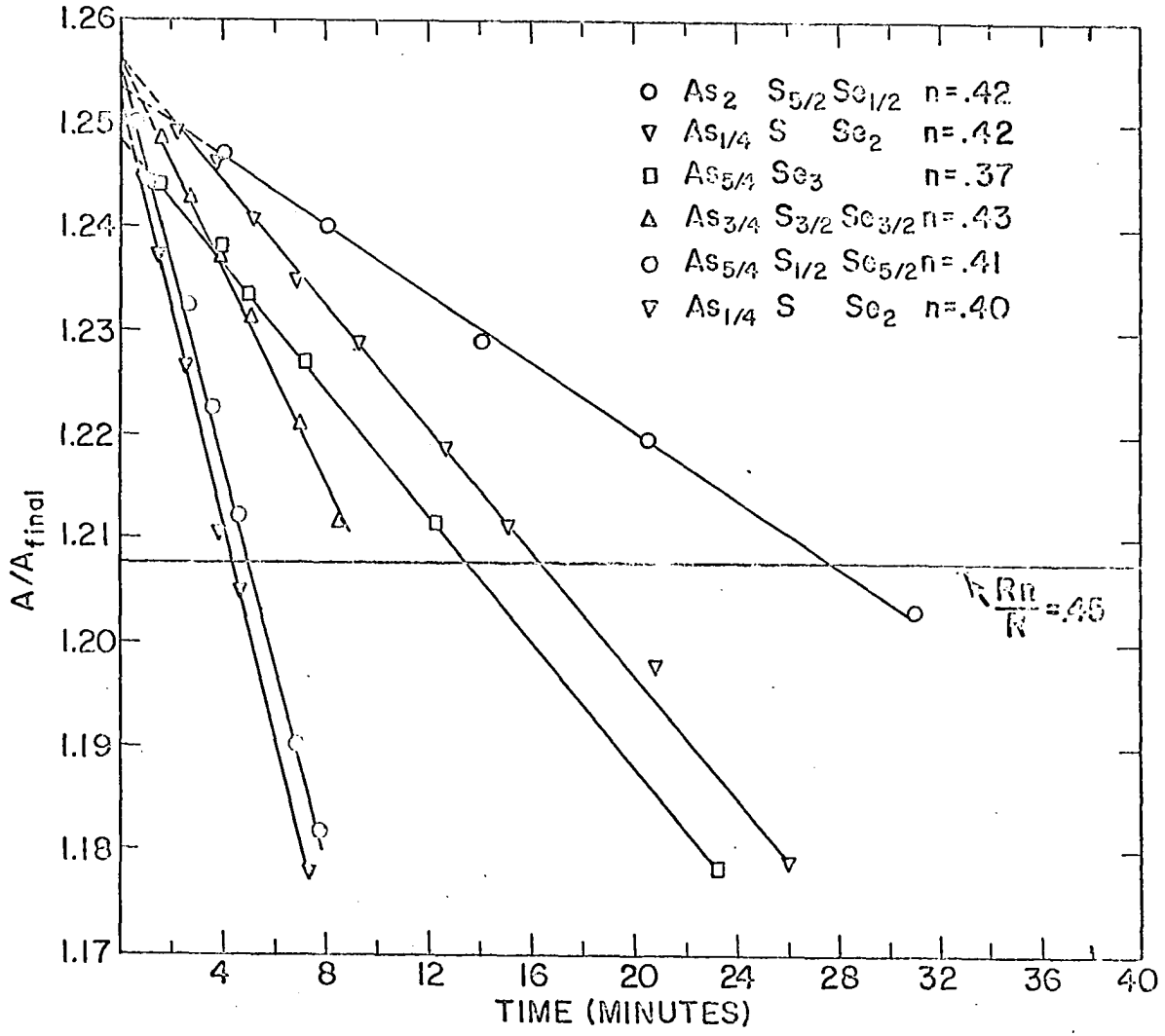

Figure 17. A/Af versus time for compositions having n-values of 0.37-0.43

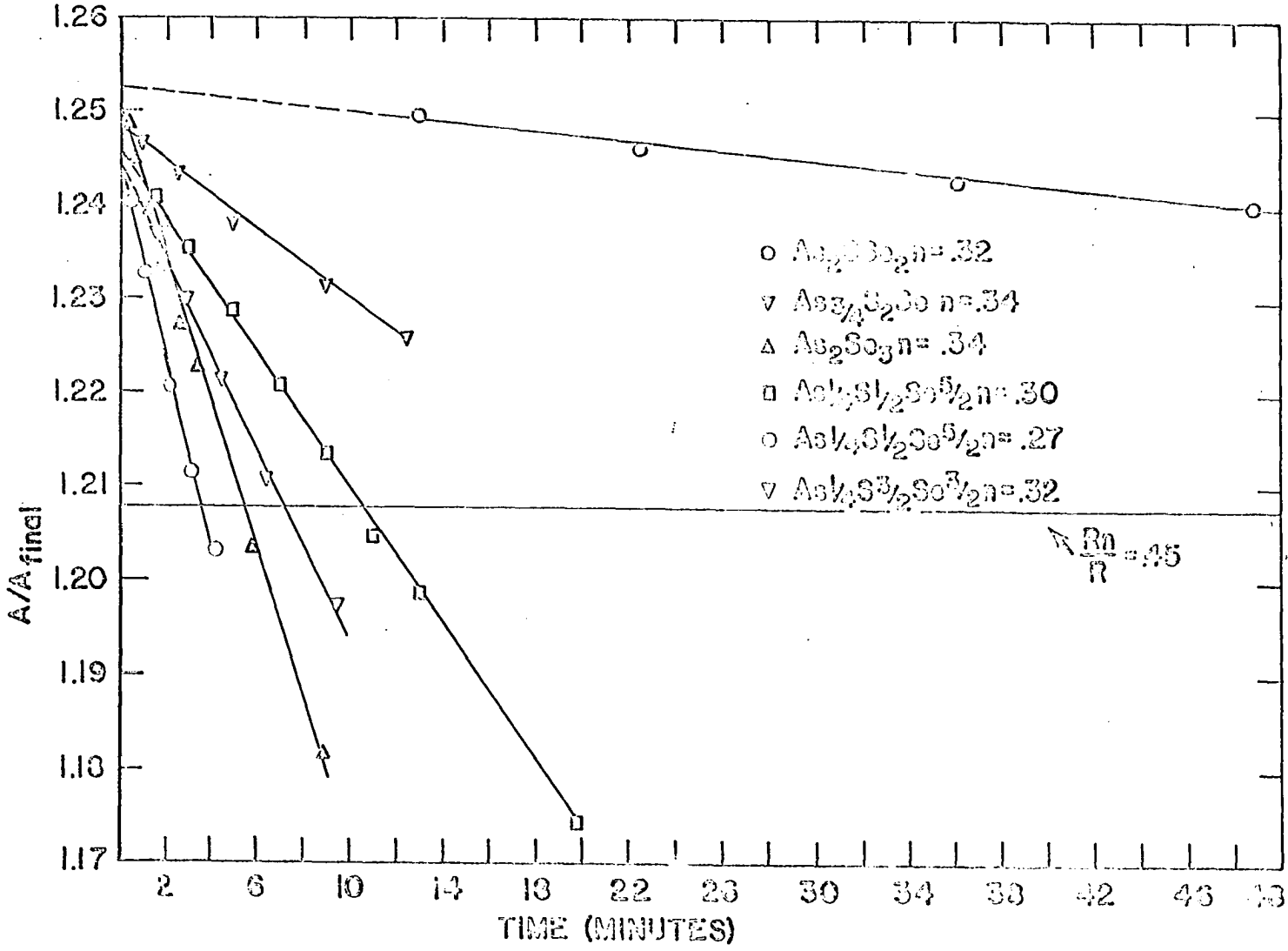

Figure 18. A/Af versus time for compositions having n-values of 0.27-0.34

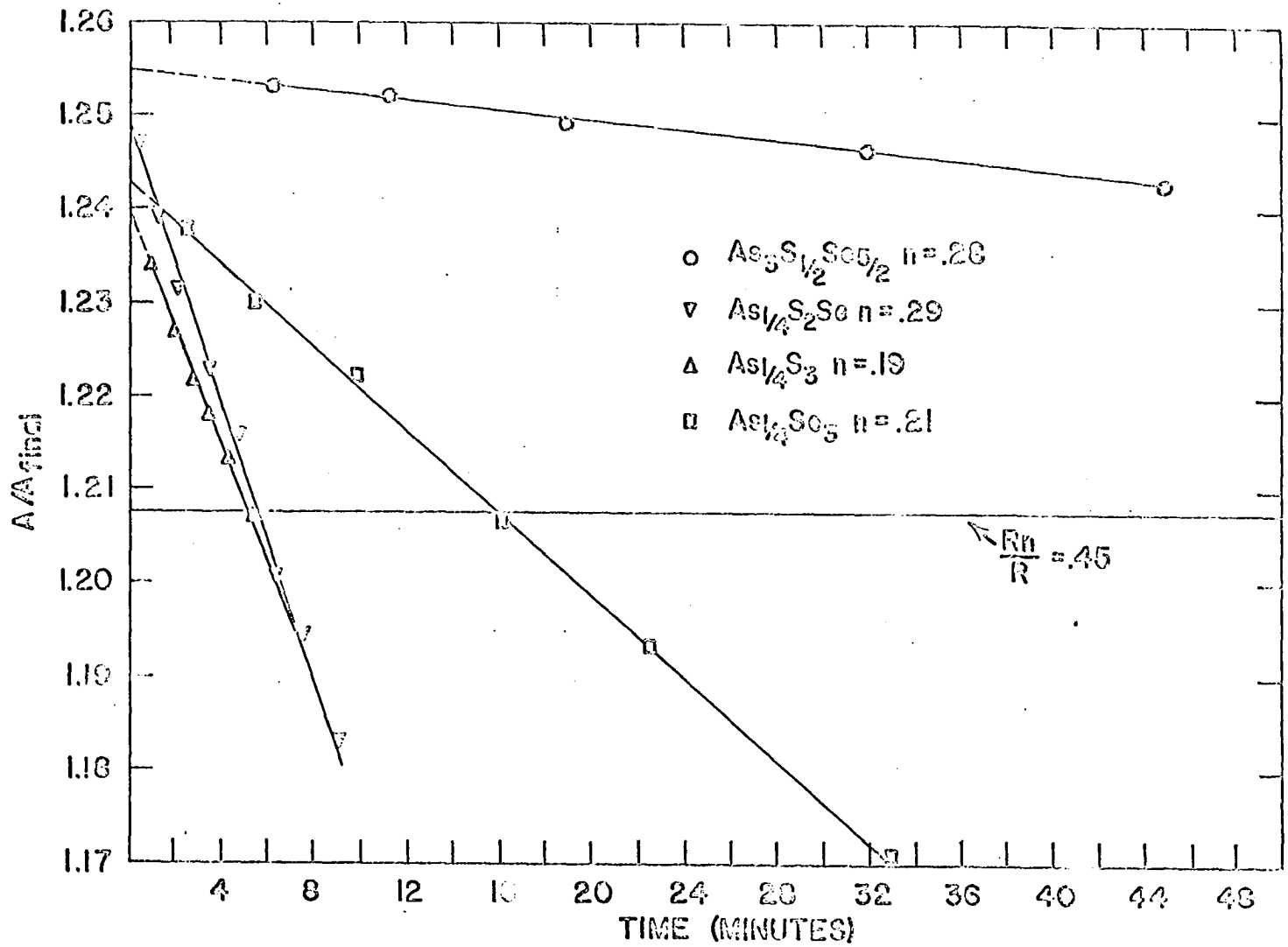

Figure 19. A/A_f versus time for compositions having n-values of 0.19-0.28

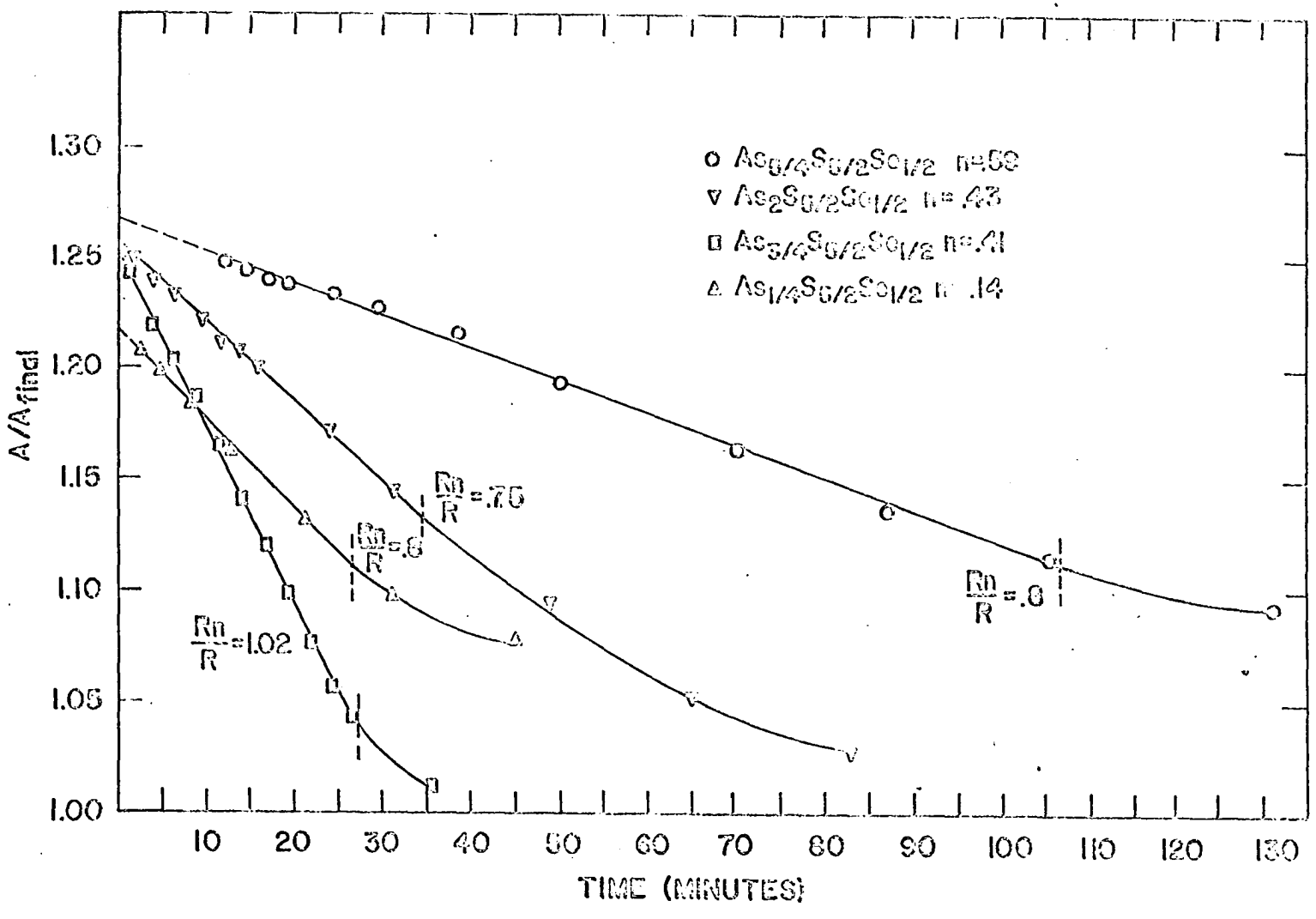

Figure 20. A/Af versus time for compositions $As_xS_{5/2}Se_{1/2}$ where x has values of 2, 5/4, 3/4 and 1/4

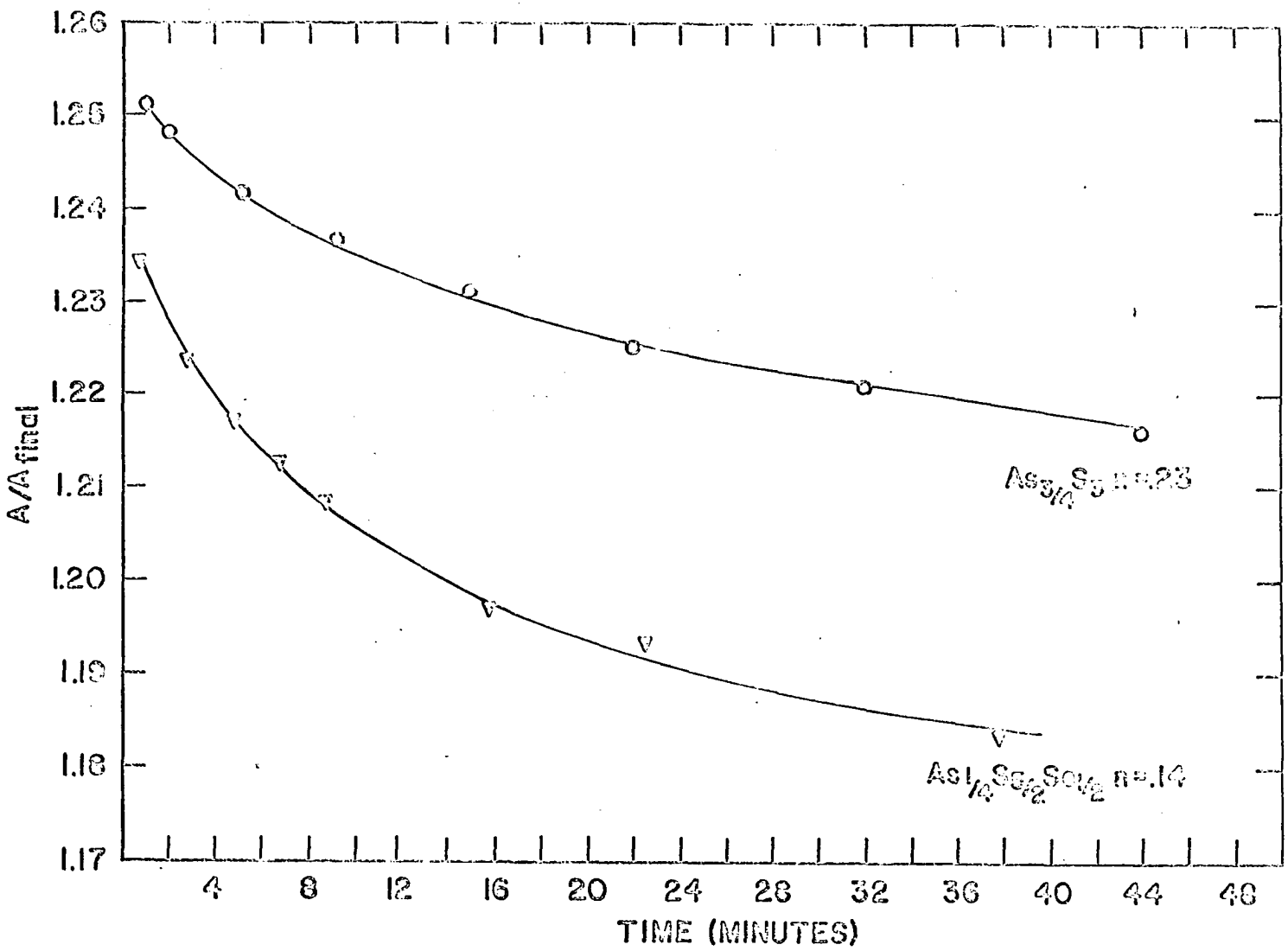

Figure 21. A/A_f versus time for $As_{3/4}S_3$ and $As_{1/4}S_{5/2}Se_{1/2}$

ANALYSIS OF RESULTS

Logarithm R_n/R_i Plotted Against Logarithm Time

It is a peculiarity of sphere-sphere sintering experiments for a given element, compound, or glass that the straight line relationships of log R_n/R_i versus log time have identical slopes when carried out at different temperatures. For the sintering of sodium silicate glass spheres Kuczynski (24) calculated that at the temperature range of his experiments, the viscosity varied from 10^{10} to 10^7 poises. In the work done by Kingery and Berg (7) and Kuczynski (24) for a sodium silicate glass the slope was 0.5; i.e., $R_n/R_i = kt^{0.5}$. This has been the accepted value which has represented all vitreous sintering by a viscous flow mechanism.

The temperatures at which the sintering experiments were run in the As-S-Se system are shown on Figure 22. All sintering experiments in the As-S-Se vitreous system investigated proceeded by a viscous flow mechanism. This statement can be made since x-ray investigations before and after sintering gave no evidence of crystallization. It is proposed that an atom-diffusion process would indeed lead to crystallization since this would be the lowest free energy condition.

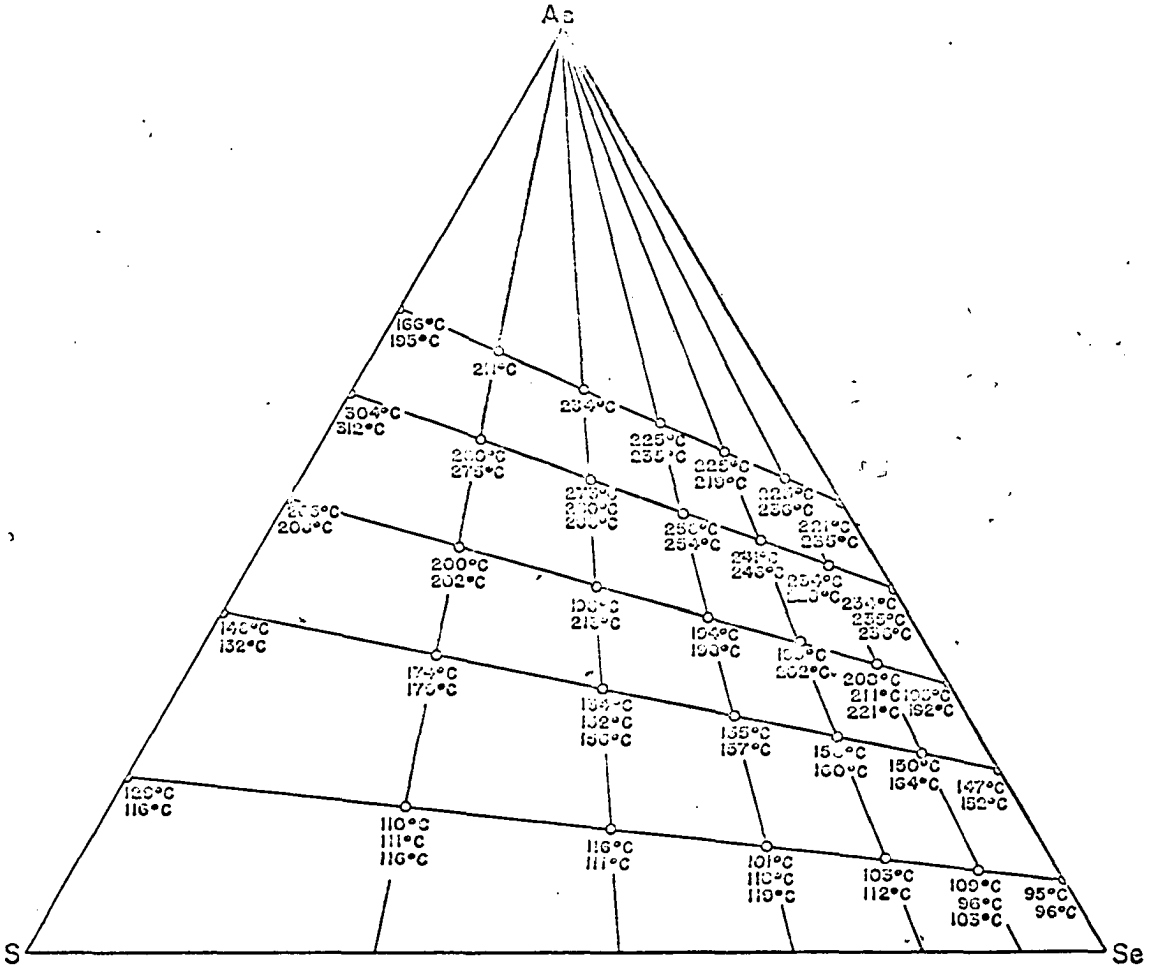

Figure 22. Weight per cent diagram of the As-S-Se system showing the temperatures at which the compositions were sintered

From the viscosity data published by Nemilov and Petrovskii (56) on the binary As-Se system, the temperatures at which the sintering data was obtained for As_2Se_3, $As_{5/4}Se_3$, $As_{3/4}Se_3$, and $As_{1/4}Se_3$ indicate that all of the experiments were done in the viscosity range of 10^7-$10^{7.5}$ poises. The viscosity for the composition As_3Se_3 ranged from $10^{7.5}$-$10^{8.5}$ poises--an increase in temperature for lower viscosities led to large volatilization losses. Since the temperature range for the sintering experiments for other compositions was chosen in the same manner as that for the As_xSe_3 region of the As-S-Se ternary, it was assumed that all of the sintering experiments in the As-S-Se ternary were done in a viscosity range of approximately $10^{6.5}$-$10^{8.5}$ poises.

For any given composition the slope of logarithm R_n/R_i plotted against logarithm time for initial sintering did indeed remain constant. Values of the slope varied from 0.12-0.65 depending on the composition of the glass. Figures 10-14 represent these slopes over the entire range of the As-S-Se vitreous system that was studied. Figure 14 represents compounds of the form $As_3(S,Se)_3$, most of which produced considerable volatilization losses in the temperature range investigated.

One might presuppose that similar compositional formulas; i.e., $As_x(S,Se)_y$, would lead to similar glass structures in the As-S-Se ternary system. If the preceding statement were true, sulfur and selenium would have to react chemically in an identical way with arsenic. Further, one would expect that glass structures with a given $As_a(S,Se)_b$ composition, where a and b are constants, would flow in the same manner in a sintering experiment such as the one performed. If the slope of logarithm R_n/R_i plotted against logarithm time were dependent on the internal structure we would expect that all glasses with a given $As_a(S,Se)_b$ composition would have an identical slope. Figure 23 shows glass compositions having the same type of structure based on similar flow characteristics. It can be seen that the slopes follow in a general pattern the $As_a(S,Se)_b$ compositional lines. Deviations are present, and this is to be expected since the chemical nature of sulfur and selenium are somewhat different.

It is proposed that the slope of logarithm R_n/R_i plotted against logarithm time is indeed structurally dependent, and the following internal structures will be proposed for those compositions representing certain slope ranges.

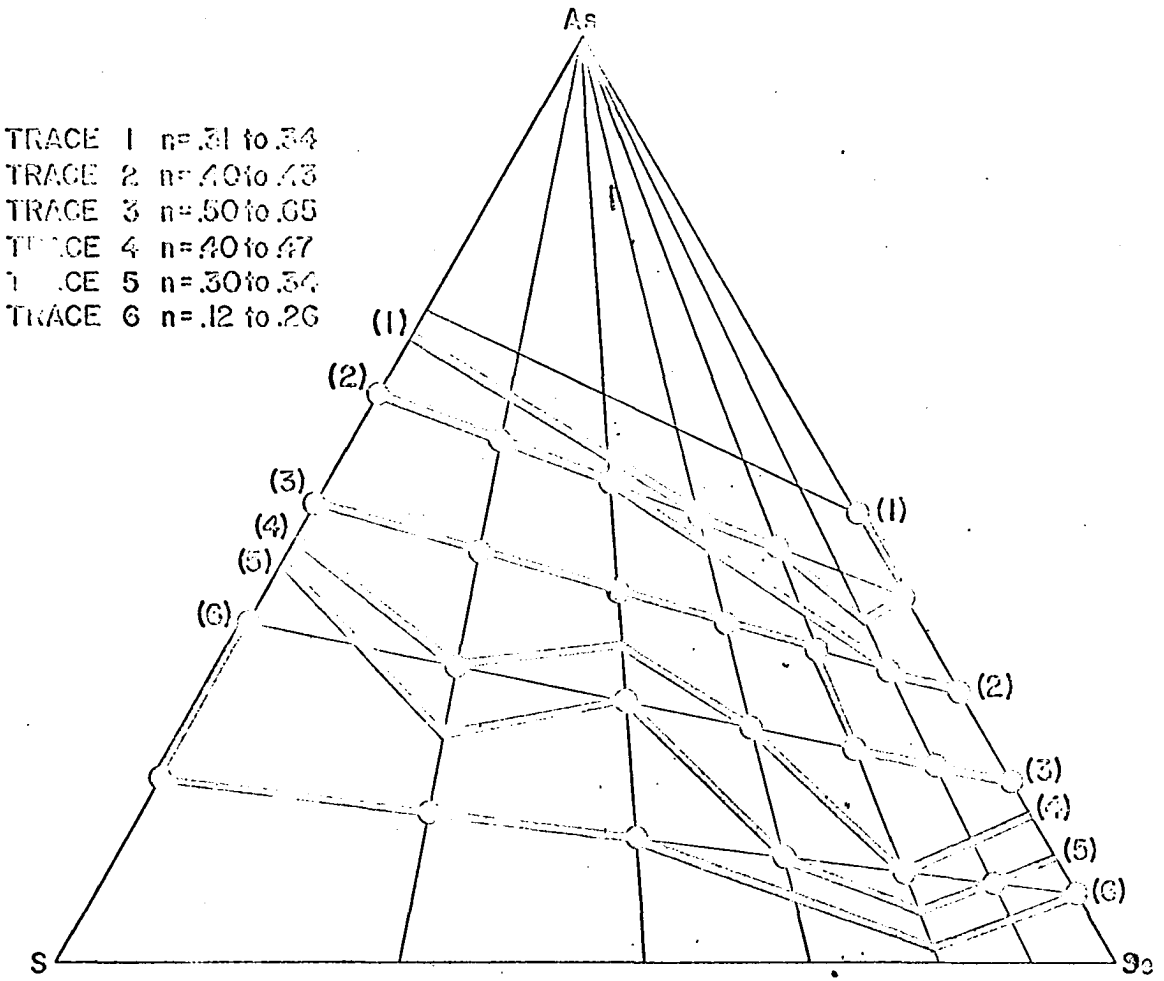

Figure 23. Compositions with similar n-values are connected where n is the slope of logarithm R_n/R_i plotted against logarithm time

Trace 6 on Figure 23

Since elemental glassy sulfur and selenium have a coordination number of two, it is not surprising that a binary glass system of sulfur and selenium exists in the form of randomly dispersed rings and chains. An arsenic addition gives rise to covalent bonds between arsenic and three sulfur and/or selenium atoms. Hence, we have introduced into a system of chains and rings trigonal "pinning points". Since elemental sulfur has been found by Eisenburg (41) to consist of chain units an order of magnitude greater than that of elemental selenium at any given temperature above the melting point of selenium, 218°C, up to 327°C, it is possible that the longer chains continue to higher arsenic levels in the high sulfur containing glasses. The fact that trace 6 includes $As_3/_4S_3$ might be resolved from this difference between sulfur and selenium. Such structures would have a viscosity dependent on the S-S, S-Se, and/or Se-Se linkages; i.e., these bonds would be involved in the activation process of viscous flow. Units involved in the flow at low viscosities would probably be small chain-like configurations.

Trace 3 on Figure 23

At 25 atom per cent arsenic the glass of composition $AsSe_3$ could theoretically be present with all trigonal $AsSe_3$ elements bound together by Se bonds.

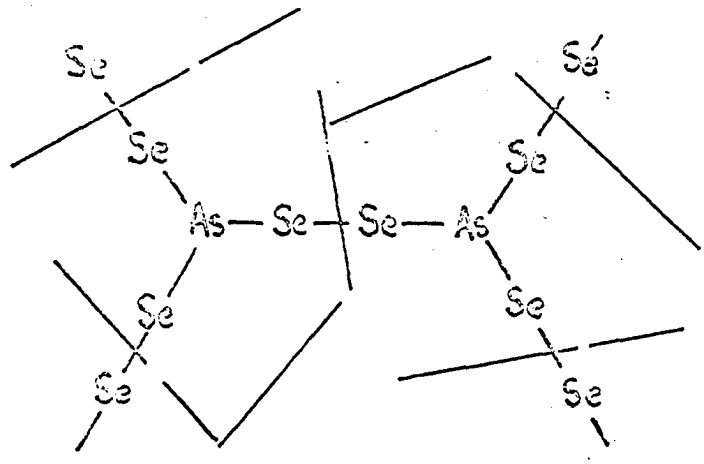

Figure 24. Trigonal $AsSe_3$ elements bound together by Se bonds

$As_{3/4}Se_3$ contains 20 atom per cent arsenic, and therefore one could expect a structure similar to that shown in Figure 24 with some longer selenium linkages present. $As_{5/4}S_3$ contains 30 atom per cent arsenic, and it is on the same trace with $As_{3/4}Se_3$. It is proposed that this trace represents trigonal elements bound together by sulfur or selenium, and no longer are there rings or chains of sulfur

or selenium present. Since sulfur does have a stronger affinity for being in long chains, it is possible that more arsenic is needed to approach this structure. At any rate S-S, S-Se, and Se-Se linkages should again be the dominant bonds involved in the activation process of viscous flow. Units involved in the flow process for compositions represented by this trace could therefore consist of small regular units, which together with a rather open structure might be the reason why the slope values for these compositions are the greatest in the entire As-S-Se ternary.

Trace 1 on Figure 23

The As_2Se_3 glass structure has been shown to be the most dense in the As-Se system. Physical measurements (57) have shown that the internal structure is indeed a continuous network characterized by As-Se bonds. This structure has no Se-Se bonds. It is postulated that due to the denseness of such a network structure and to the disappearance of Se-Se bonds that the slope values have again become lower. Vaipolin and Porai-Koshits (54) have shown that the coordination of selenium to arsenic is greater than sulfur to arsenic in the compositions As_2Se_3 and As_2S_3. This would cause this selenium rich glass to be the densest in the entire As-S-Se ternary.

Traces 2,4,5 on Figure 23

It is postulated that these structures are hybrids between those described above, and their slope values should fall between those of the structures that have been explained.

A/A_f Plotted Against Time

Figures 16-20 show the relationship between surface area and time for the sintering experiments done in the vitreous As-S-Se system. These relationships are shown to be of the form

$$A/A_f = -k_1 t + k_2 \qquad (9)$$

where A is the surface area of the two sintering spheres at any elapsed time, t; A_f is the surface area finally obtained; and k_1 and k_2 are constants.

The initial area is the surface of two spheres of radii R_i. The final area is the surface of one sphere of radius $2^{1/3}R_i$. The ratio of A_i/A_f is therefore 1.26. The excess surface area, $A_i - A_f$, coupled with its surface energy, is the driving force for the sintering process. Sintering will continue as long as a relatively low viscosity is present for the flow mechanism to occur and as long as the total surface, A, is greater than A_f.

It is significant that a straight line relationship

exists between surface area and time. Such a relationship shows that the excess free energy decreases at a constant rate. This in turn implies that the internal energy must be dissipated at a constant rate. When adjacent layers of fluid are moving past one another, these motions are resisted by a shearing force which tends to reduce their relative velocity. It seems reasonable to assume that a certain reproducible type of internal flow pattern would have to be present to cause the well defined neck radius versus length pattern shown in Figure 7. It is proposed that a well defined, constant valued internal velocity exists, during the period when the flow is described by Equation 9, which contributed to the constant dissipation of energy. No prediction will be made regarding this particular flow pattern which exists during this viscous flow process.

In Equation 9 the constant k_1 depends on temperature, and the constant k_2 depends on the composition. Compositions that had similar slopes of logarithm R_n/R_i plotted against logarithm time had similar intersects on the A/A_f axis as shown in Figures 16-20. The sintering data which gave slopes above 0.5 for logarithm R_n/R_i plotted against logarithm time had an "ideal" value for their intersection. These equations were

of the form

$$A/A_f = -k_1 t + 1.26 \qquad (10)$$

which could also be written

$$A = A_i - k_1 t \qquad (11)$$

where A_i is the initial area of the two spheres. The value of 1.26 represents the fact that flow, which gave a constant surface area versus time relationship, started with initial contact of the spheres; i.e., with the initial area. The data show that the intersections, represented by k_2, are associated with the traces shown on Figure 23; i.e., the intersection is compositionally dependent. An intersection below 1.26 represents a situation where the initial neck growth occurred rapidly. After this event a flow pattern could be developed in which the surface area versus time relationship could become constant.

Figure 20 shows the sintering data for the compositions $As_xS_{5/2}Se_{1/2}$, where x takes on values of 2, 5/4, 3/4, and 1/4. Note that with decreasing slope values for logarithm R_n/R_i plotted against logarithm time the intersections on the A/A_f axis decrease. It is also significant that the constant surface area versus time relationship exists far beyond the initial sintering as shown in Figure 20.

Figure 21 shows that the data for sintering of long chain compositions at viscosities above approximately $10^{7.5}$ poises does indeed involve viscoelastic relationships as predicted by Lontz (29). It is presumed that chain entanglement did occur which inhibited the flow process.

It should be acknowledged that sintering expressions using the driving force for sintering as the excess surface energy over some value which would be attained finally at the temperature under consideration have been developed by Nicholson and Gregg (58,59) for crystalline systems. Nicholson supports the relationship

$$dA/dt = -k_s(A-A_f) \qquad (12)$$

where k_s is a constant which depends on the temperature, and A_f is the surface area finally attained. Gregg proposes that the empirical equation

$$dA/dt = -k_s A t^{-m} \qquad (13)$$

is a convenient way of describing the sintering process, where m is greater than zero and less than one.

Shrinkage Against Time

Kingery and Berg (7) and Kubo (20) have reported that the linear shrinkage for the sintering of spherical glass particles of sodium silicate glass follows the relationship

$$(\Delta L/L)^{5/2} = kt \qquad (5)$$

where L is the distance between the centers of the two initial spheres, ΔL is the shrinkage, k is a constant which depends on temperature, and t is the elapsed time.

If we take the relationship of A/A_f versus $\Delta L/L$ for the constant radii model (Appendix B.2.), the relationship

$$A/A_f = 1.26 - 2.11(\Delta L/L) + 7.317(\Delta L/L)^2 - 13.075(\Delta L/L)^3 \qquad (14)$$

exists. Substitution of $A/A_f = -k_1 t + 1.26$ for compositions where the slope of logarithm R_n/R_i plotted against logarithm time is greater than 0.5, gives the following shrinkage equation

$$-k_1 t = -2.11(\Delta L/L) + 7.317(\Delta L/L)^2 - 13.075(\Delta L/L)^3 \qquad (15)$$

where L is the initial diameter of the two spheres, $4R_i$; ΔL is the linear shrinkage at any elapsed time, t; and k_1 is a constant which depends on the temperature. (Equation 14 was also obtained using a least square computer program for the best cubic fit.)

CONCLUSIONS

1. For the sintering of vitreous spheres in the As-S-Se system the slope of logarithm R_n/R_i plotted against logarithm time is compositionally dependent, where R_n is the radius of the contact neck between the two sintering spheres and R_i is the initial radius of either sphere. Three main types of internal structure are proposed in order of increasing arsenic content: a) A system of chains and ring structures with arsenic "pinning points". b) Trigonal $As(S,Se)_3$ elements bound together by S-S, S-Se, and/or Se-Se linkages. c) A dense network consisting of entirely As-S and/or As-Se linkages. Vitreous compositional structures existing between the three main types consist of combinations of those considered. Initial slopes of logarithm R_n/R_i plotted against logarithm time varied from 0.12-0.65, therefore no one value should be used to represent the viscous flow mechanism.

2. Surface area versus time relationships are shown to be of the form

$$A/A_f = -k_1 t + k_2$$

where k_1 is a constant which depends on the temperature and k_2 is a constant which depends on the composition (i.e., depends on internal glass structure). This equation indi-

cates a constant dissipation of internal energy by the flow process.

3. Viscoelastic properties come into existence at viscosities above approximately $10^{7.5}$ poises when the structure involves long chain configurations.

4. A linear shrinkage equation of the form

$$-k_1 t = -2.11(\Delta L/L) + 7.317(\Delta L/L)^2 - 13.075(\Delta L/L)^3$$

was obtained for compositions whose slopes of logarithm R_n/R_i plotted against logarithm time were greater than 0.5; where L is the initial diameter of the two spheres, $4R_i$; ΔL is the linear shrinkage at any elapsed time, t; and k_1 is a constant which depends on temperature.

LITERATURE CITED

1. Gray, T. J. The defect solid state. New York, N.Y., Interscience Publishers, Inc. 1957.

2. Kingery, W. D. Introduction to ceramics. New York, N.Y., John Wiley and Sons, Inc. 1960.

3. Oel, H. J. The relationship between free energy and kinetics in sintering processes. In Kingery, W. D., ed. Kinetics of high-temperature processes. pp. 179-186. New York, N.Y., John Wiley and Sons, Inc. 1959.

4. Thummler, F. Recent work on the theory of sintering in the German Democratic Republic. Powder Metallurgy. 1. No. 3: 125-145. 1959.

5. Jones, W. D. Fundamental principles of powder metallurgy. London, England, Edward Arnold (Publishers), Limited. 1960.

6. Walker, R. F. Mechanism of material transport during the sintering of powders. American Ceramic Society Journal 38: 187-197. 1955.

7. Kingery, W. D. and Berg, M. Study of the initial stages of sintering solids by viscous flow, evaporation-condensation, and self-diffusion. Journal of Applied Physics 26: 1205-1212. 1955.

8. Geach, G. A. The theory of sintering. Progress in Metal Physics 4: 174-204. 1953.

9. Burke, J. E. Recrystallization and sintering in ceramics. In Kingery, W. D., ed. Ceramic fabrication processes. pp. 120-131. New York, N.Y., John Wiley and Sons, Inc. 1958.

10. Leszynski, W. Powder metallurgy. New York, N.Y., Interscience Publishers, Inc. 1961.

11. Wilder, D. R. Sintering mechanism as applied to refractory oxides: a bibliography, 1937-1952. U.S. Atomic

Energy Commission Report ISC-288 [Ames Lab., Ames, Iowa.] 1956.

12. Wilder, D. R. Sintering mechanism as applied to refractory oxides: a bibliography. Supplement 1, 1952-1955. U.S. Atomic Energy Commission Report ISC-288 [Ames Lab., Ames, Iowa.] 1956.

13. Wilder, D. R. Sintering mechanism as applied to refractory oxides: a bibliography. Supplement 2, 1955-1959. U.S. Atomic Energy Commission Report ISC-288 [Ames Lab., Ames, Iowa.] 1960.

14. Goetzel, C. G. Treatise on powder metallurgy. Vol. 3. Classified and annotated bibliography. New York, N.Y., Interscience Publishers, Inc. 1953.

15. Goetzel, C. G. Treatise on powder metallurgy. Vol. 4. Classified and annotated bibliography, 1950-1960. Part 1. Literature survey. New York, N.Y., Interscience Publishers, Inc. 1963.

16. Nemilov, S. V. The interrelationship between the activation entropy of viscous flow, heat capacity, and valence structure of glass. Journal of Applied Chemistry of the U.S.S.R. 37. No. 2: 306-312. 1964.

17. Nemilov, S. V. and Petrovskii, G. T. Calculation and study of the energy parameters of the viscosity in the Se-As system. Journal of Applied Chemistry of the U.S.S.R. 36. No. 9: 1853-1858. 1963.

18. Frenkel, J. Viscous flow of crystalline bodies under action of surface tension. Journal of Physics 9. No. 5: 385-391. 1945.

19. Kuczynski, G. C. Theory of solid state sintering. In Leszynski, W., ed. Powder metallurgy. pp. 11-29. New York, N.Y., Interscience Publishers, Inc. 1961.

20. Kubo, T., Shinriki, K. and Kutaka, K. Shrinkage of powder compacts during sintering. Kogyo Kagku Zasshi 61: 918-922. 1958.

21. Johnson, D. L. and Cutler, I. B. Diffusion sintering. I. Initial stage sintering models and their application to shrinkage of powder compacts. American Ceramic Society Journal 46: 541-544. 1963.

22. Johnson, D. L. and Cutler, I. B. Diffusion sintering. II. Initial sintering kinetics of alumina. American Ceramic Society Journal 46: 545-550. 1963.

23. Johnson, D. L. and Clarke, T. M. Grain boundary and volume diffusion in the sintering of silver. Acta Metallurgica 12: 1173-1179. 1964.

24. Kuczynski, G. C. Study of the sintering of glass. Journal of Applied Physics 20: 1160-1163. 1949.

25. Mackenzie, J. K. and Shuttleworth, R. A phenomenological theory of sintering. Physical Society (London) Proceedings 62: 833-852. 1949.

26. Clark, P. W. and White, J. Some aspects of sintering. British Ceramic Society Transactions 49: 305-333. 1950.

27. Clark, P. W., Cannon, J. H. and White, J. Further investigations on the sintering of oxides. British Ceramic Society Transactions 52: 1-49. 1953.

28. Brinkman, H. C. Problems of fluid flow through swarms of particles and through macromolecules in solution. In Proceedings International Rheological Congress Holland 1948. Amsterdam, Holland, North-Holland Publishing Company. 1949.

29. Lontz, J. F. Sintering of polymer materials. In Bonis, L. J. and Hausner, H. H., eds. Fundamental phenomena in the material sciences. pp. 25-47. New York, N.Y., Plenum Press. 1964.

30. Kirby, P. L. Kinetics of mechanical relaxation processes in inorganic glasses. In Frechette, V. D. Non-crystalline solids. pp. 269-294. New York, N.Y., John Wiley and Sons, Inc. 1960.

31. Warren, B. E. X-ray diffraction study of the structure of glass. Chemical Review 26: 237-255. 1940.

32. Zachariasen, W. H. On the structure of vitreous oxides. Physical Review 39: 185. 1932.

33. Stanworth, J. E. The structure of glass. Glass Technology Society Journal 137: 54-67. 1946.

34. Huggins, M. L., Sun, K. H. and Silverman, A. The vitreous state. American Ceramic Society Journal 26: 393-394. 1943.

35. Sun, K. H. Glass-forming substances. Glass Industries 27: 552. 1946.

36. Van Wazer, J. R. Phosphorus and its compounds. New York, N.Y., Interscience Publishers, Inc. 1961.

37. Mackenzie, J. D., ed. Modern aspects of the vitreous state. Washington, D.C., Butterworths. 1960.

38. Frechette, V. D. Non-crystalline solids. New York, N.Y., John Wiley and Sons, Inc. 1960.

39. Prins, J. A. Amorphous sulfur and selenium. In Frechette, V. D. Non-crystalline solids. pp. 322-327. New York, N.Y., John Wiley and Sons, Inc. 1960.

40. Zachariasen, W. H. Atomic arrangement in glass. American Chemical Society Journal 54: 3841-3851. 1932.

41. Eisenburg, A. and Tobolsky, A. V. Equilibrium polymerization of selenium. Journal of Polymer Science 46: 19-29. 1960.

42. Tobolsky, A. V. and Eisenburg, A. Equilibrium polymerization of sulfur. American Chemical Society Journal 81: 780-782. 1959.

43. Fairbrother, F., Gee, G. and Merrall, G. T. Polymerization of sulfur. Journal of Polymer Science 16: 459-469. 1955.

44. Bradley, A. J. The crystal structures of the rhombohedral forms of selenium and tellurium. Philosophical Magazine 48: 477-496. 1924.

45. Tobolsky, A. V., Owen, G. D. T. and Eisenberg, A. Viscoelastic properties of S-Se-As copolymers. Journal of Colloid Science 17: 717-725. 1962.

46. Flaschen, S. S., Pearson, A. D. and Northover, W. R. Formation and properties of low-melting glasses in the ternary systems As-Tl-S, As-Tl-Se, and As-Se-S. American Ceramic Society Journal 43: 274-278. 1960.

47. Vaipolin, A. A. and Porai-Koshits, E. A. The structure of glassy arsenic chalcogenide. Corrections to the radial distribution curves. Soviet Physics Solid State 5. No. 1: 178-185. 1963.

48. Petz, J. I., Kruh, R. R. and Amstutz, G. C. X-ray diffraction study of lead sulfide-arsenic sulfide glasses. Journal of Chemistry and Physics 34: 526-529. 1961.

49. Hopkins, T. F., Pasternak, R. A., Gould, E. S. and Herndon, J. R. X-ray diffraction study of arsenic trisulfide-iodide glasses. Journal of Physical Chemistry 66: 733-736. 1962.

50. Vaipolin, A. A. and Porai-Koshits, E. A. Structure models of glasses and structure of crystalline chalcogenides. Soviet Physics Solid State 5. No. 2: 497-500. 1963.

51. Vaipolin, A. A. and Porai-Koshits, E. A. The structure of arsenic chalcogenide glasses. Vitreous and crystalline states in the As_2Se_3-As_2Te_3 system. Soviet Physics Solid State 5. No. 1: 186-190. 1963.

52. Vaipolin, A. A. and Porai-Koshits, E. A. X-ray study of vitreous arsenic chalcogenides. In Structure of glass, Proc. All-Union Conf. 3rd, Leningrad, 1959 pp. 423-425. Academy of Sciences U.S.S.R. Press Moscow-Leningrad. 1960.

53. Kolomiets, B. T. and Pozdnev, V. P. Vitreous semiconductors. VII. Viscosity of vitreous semiconductors of the As_2S_3-As_2Te_3 system. Soviet Physics Solid State 2. No. 1: 23-29. 1960.

54. Vaipolin, A. A. and Porai-Koshits, Y. A. The structure of vitreous arsenic chalcogenides. Soviet Physics Solid State 2. No. 7: 1500-1508. 1960.

55. Nemilov, S. V. Viscosity and structure of glasses in the selenium-germanium system. Journal of Applied Chemistry of the U.S.S.R. 37. No. 5: 1026-1030. 1964.

56. Nemilov, S. V. and Petrovskii, G. T. An investigation of the viscosity of glasses of the selenium-arsenic system. Journal of Applied Chemistry of the U.S.S.R. 36. No. 5: 932-935. 1963.

57. Borisova, Z. U. Effect of some elements on the electrical conductivity and microhardness of the glassy arsenic selenide. Akademiia Nauk SSSR Izvestiia, Seriia Fizicheskaia. 28. No. 8: 1293-1294. 1964.

58. Nicholson, D. Variation of surface area during the thermal decomposition of solids. Faraday Society Transactions 61: 990-998. 1965.

59. Gregg, S. J., Packer, R. K. and Wheatly, K. H. The production of active solids by thermal decomposition. Part V. The sintering of active magnesium oxide. Chemical Society London Journal 1: 46-50. 1955.

APPENDIX A

The heater control unit used to provide a constant temperature for the sintering experiments is shown schematically in Figure A.1.

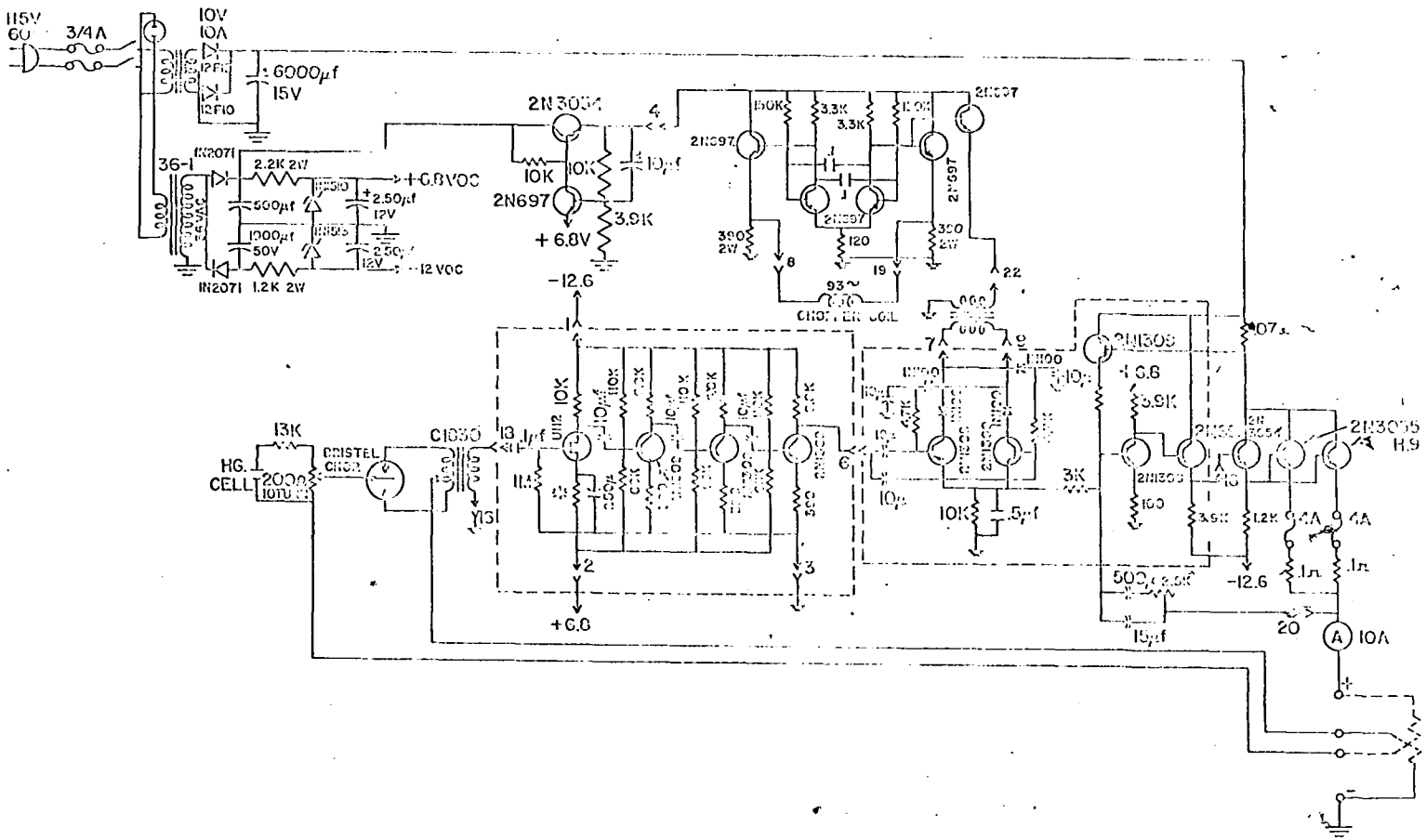

Figure A.1. Heater control unit to provide constant temperature

APPENDIX B

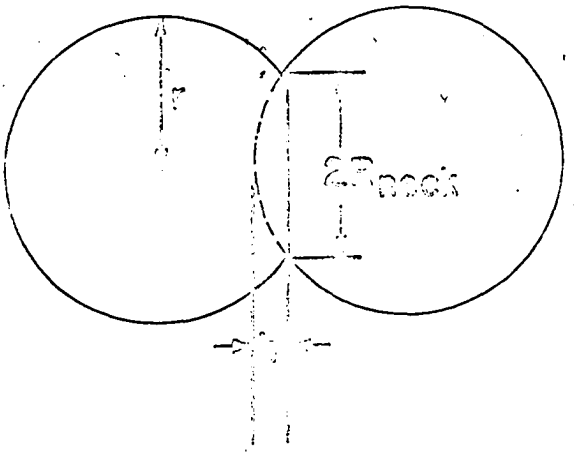

$$\frac{4\pi r^3}{3} - \frac{\pi h^2}{3}(3r-h) = \frac{4}{3}\pi 10^3$$

$$r^3 - \frac{h^2}{4}(3r-h) = 10^3$$

$$r^3 - \left[\frac{3h^2}{4}\right] r - \left[10^3 \; \frac{-h^3}{4}\right] = 0$$

which is of the form $r^3 + ar + b = 0$

solution is of the form $r = A_1 + B_1$ where:

$$A_1 = \left[-\frac{b}{2} + \left[\frac{b^2}{4} + \frac{a^3}{27}\right]^{\frac{1}{2}}\right]^{1/3}$$

$$B_1 = \left[-\frac{b}{2} - \left[\frac{b^2}{4} + \frac{a^3}{27}\right]^{\frac{1}{2}}\right]^{1/3}$$

also

$$R_n^2 = (r^2 - (r-h)^2)$$

Model B.1. Radii increasing model

h	A_1	B_1	$r=A_1+B_1$	$-2(2\pi rh)$ $+2(4\pi r^2)$	A/A_f	$\frac{R_{neck}}{R_{initial}}$	$\frac{Length}{Length_{initial}}$
1/4	0.016	9.9999	10.004	2483.862	1.2450	0.2240	0.9879
1	0.027	9.999	10.026	2400.383	1.2032	0.4365	0.9526
2	0.100	9.993	10.093	2306.588	1.1562	0.6031	0.9093
3	0.229	9.977	10.206	2233.125	1.1193	0.7227	0.8706
4	0.402	9.946	10.348	2171.097	1.0882	0.8172	0.8348
5	0.632	9.894	10.526	2123.269	1.0643	0.8959	0.8026
6	0.917	9.814	10.731	2085.042	1.0451	0.9632	0.7731
8	1.678	9.536	11.214	2033.193	1.0191	1.0743	0.7214
10	2.778	8.998	11.776	2005.447	1.0052	1.1641	0.6776
12	4.636	7.767	12.403	1995.946	1.0005	1.2343	0.6403

Model B.1. Radii increasing model

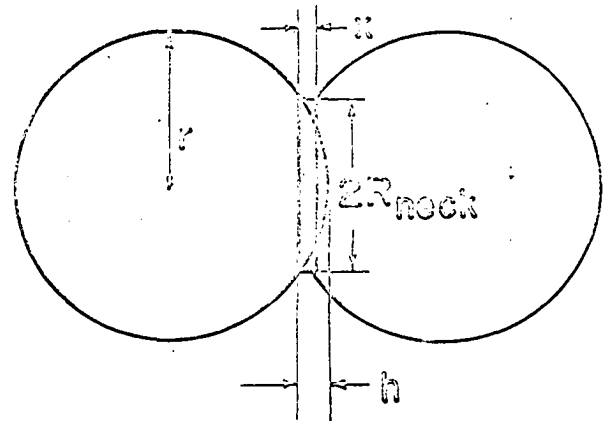

$$2\left[\frac{\pi h^2}{3}(30-h)\right] = X(\pi R_n^2)$$

also $R_n^2 = 10^2 - (10-h)^2$

Model B.2. Radii remaining constant model. The sphere segments become cylinder

h	$\frac{R_{neck}}{R_{initial}}$	X	$\frac{Length}{Length_{initial}}$	$2(4\pi 10^2)-2(2\pi 10h)$ $+2\pi R_n X$	A/A_f
1/8	0.158	0.1252	0.99688	2498.55	1.252
1/2	0.312	0.504	0.98760	2460.33	1.233
1	0.436	1.018	0.97545	2415.51	1.210
3/2	0.527	1.540	0.96350	2375.76	1.191
2	0.600	2.074	0.95185	2340.13	1.173
5/2	0.661	2.620	0.94050	2307.93	1.157
3	0.714	3.176	0.92940	2278.77	1.142
7/2	0.760	3.748	0.91870	2251.44	1.129
4	0.800	4.334	0.90835	2228.49	1.117
9/2	0.835	4.936	0.89840	2206.75	1.106
5	0.866	5.556	0.88895	2187.28	1.096
10	1.000	13.334	0.83335	2094.41	1.050

Model B.2. Radius remaining constant model

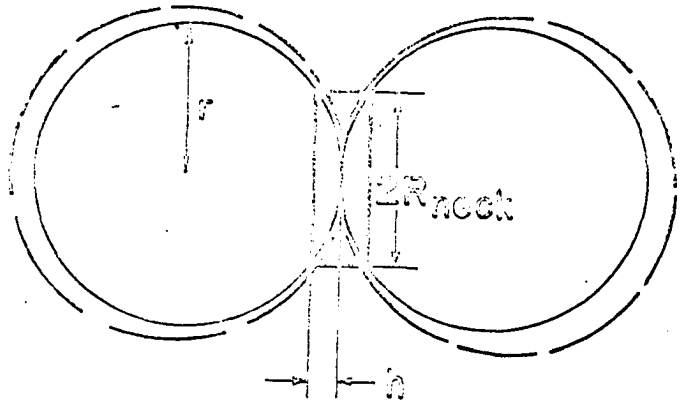

$$\frac{4}{3}\pi 10^3 = \frac{4}{3}\pi r^3 - \frac{\pi h^2}{3}(3r-h) + \pi R_n{}^2 h$$

$$\frac{4}{3}\,10^3 = \frac{4}{3}\,r^3 - \frac{h^2}{3}\,(3r-h) + (r^2 - (r-h)^2)h$$

$$\frac{4}{3}\,10^3 = \frac{4}{3}\,r^3 - \frac{2}{3}\,h^3 + h^2 r$$

$$\frac{2}{3}\,h^3 - rh^2 + \frac{4}{3}\,(10^3 - r^3) = 0$$

$$h^3 - \frac{3}{2}\,rh^2 + 2(10^3 - r^3) = 0$$

equation of the form $h^3 + ph^2 + qh + r_1 = 0$

$$a = \frac{1}{3}(-p^2)$$

$$b = \frac{1}{27}\,(2p^3 + 27r)$$

where: $p = -3/2r$

$q = 0$

$r_1 = 2(10^3 - r^3)$

A trigometric solution is useful

$$\cos \phi = \frac{-b}{2} \div \left[-\frac{a^3}{27}\right]^{\frac{1}{2}}$$

Model B.3. Radii decreasing model. Two whole spheres with filled in cylinder

x will have the following values:

$$\left[-\frac{a}{3}\right]^{\frac{1}{2}} \cos\frac{\phi}{3}\ ,\ \left[-\frac{a}{3}\right]^{\frac{1}{2}} \cos\left[\frac{\phi}{3}+120^{\circ}\right]\ ,\ 2\left[-\frac{a}{3}\right]^{\frac{1}{2}} \cos\left[\frac{\phi}{3}+240^{\circ}\right],$$

where $h = x - \frac{p}{3}$

Model B.3. (Continued)

r	cos ϕ	x	h	$4\pi R_{ij}h + 8\pi r^2 - 4\pi rh$		$\frac{R_{neck}}{R_{initial}}$	$\frac{Length}{Length_{initial}}$
9.283			9.283	2165.796	1.0856	0.928	0.928
9.400	$129^{o}11'$	2.1252	6.8252	2189.900	1.0977	0.904	0.940
9.500	$109^{o}19'$	1.0645	5.7895	2213.336	1.1094	0.874	0.950
9.600	$92^{o}25'$	0.1340	4.9340	2241.203	1.1234	0.839	0.960
9.700	$76^{o}26'$	-0.7639	4.0861	2272.853	1.1393	0.791	0.970
9.800	$59^{o}59'$	-1.7018	3.1982	2310.977	1.1584	0.724	0.980
9.900	$40^{o}58'$	-2.7869	2.1631	2362.055	1.1840	0.618	0.990
9.950	$28^{o}30'$	-3.4846	1.4904	2399.96	1.2030	0.524	0.995
9.98	$5^{o}75'$	-4.0671	0.9229	2436.104	1.2211	0.419	0.998
9.999	$3^{o}58'$	-4.7992	0.2003	2492.611	1.2494	0.198	0.9999

Model B.3. Radii decreasing model

APPENDIX C

The data obtained for sintering of vitreous compositions in the As-S-Se ternary are tabulated in Tables C.1. to C.35.

Table C.1. Time, neck diameter measurements, length measurements, radius ratio, and length ratio of As_3Se_3

Time (minutes:seconds)	$2R_{neck}$	$\frac{R_{neck}}{R_{initial}}$
($221^{\circ}C$; sphere diameters 205 and 206 microns; initial length 412 microns; initial sphere diameter readings 212 and 213)		
14:00	29	.136
23:00	31.5	.148
42:00	36	.169
69:00	42	.197
111:00	54.5	.256
140:00	60	.282
175:00	65.5	.308
203:00	68.5	.322
231:00	71.5	.336
257:30	74	.347
295:00	78.5	.369
330:00	80.5	.378
445:00	86.5	.406
	Length	$\frac{Length}{Length_{initial}}$
445:00	417	.977
($235^{\circ}C$; sphere diameters 196 and 196 microns; initial sphere diameter readings 202 and 202 microns)		
	$2R_{neck}$	$\frac{R_{neck}}{R_{initial}}$
20:30	44	.217
34:00	50.5	.249
53:00	54	.266
103:00	66.5	.328
151:00	87.5	.431

Table C.2. Time, neck diameter measurements, and radius ratio of As_2Se_3

(234°C; sphere diameters 198 and 198 microns; initial sphere diameter readings 205 and 205)

Time (minutes:seconds)	$2R_{neck}$	$\frac{R_{neck}}{R_{initial}}$
2:00	35	.171
3:50	41	.200
6:30	47	.230
11:30	55.5	.271
18:00	63.5	.310
27:00	71.0	.346
35:15	76	.371
58:30	95.5	.466
89:00	116.0	.565
(235°C; sphere diameters 190 and 190 microns; initial sphere diameter readings 197 and 197)		
5:45	33.5	.170
10:30	49	.249
17:05	59.5	.302
24:40	70	.355
37:15	82	.416
53:30	94	.477
66:00	101	.512
77:45	107	.542
(236°C; sphere diameters 201 and 203 microns; initial sphere diameter readings 208 and 210)		
3:00	30	.144
6:40	40.5	.194
10:30	49.5	.237
15:25	60	.287
21:15	69	.330
28:10	77.5	.371
35:35	88	.421
43:30	99	.474
59:00	110.5	.523
128:15	161.0	.770

Table C.3. Time, neck diameter measurements and radius ratio of $As_{5/4}Se_3$

Time (minutes:seconds)	$2R_{neck}$	$\frac{R_{neck}}{R_{initial}}$
(195°C; sphere diameters 210 and 211 microns; initial sphere diameter readings 217 and 218)		
1:30	44	.206
2:30	48.5	.227
3:15	55.5	.259
4:10	59	.276
5:10	64	.299
6:30	74	.346
9:50	92.5	.432
13:15	108.5	.507
22:00	150	.701
28:45	178	.832
34:10	192	.897
(192°C; sphere diameters 239 and 239 microns; initial sphere diameter readings 247 and 247)		
2:00	57.5	.233
3:50	69.0	.279
5:00	76.0	.308
7:10	86.0	.348
12:15	106.0	.429
23:15	143.0	.579
27:00	151.5	.613

Table C.4. Time, neck diameter measurements, and radius ratio of $As_3/4Se_3$

Time (minutes:seconds)	$2R_{neck}$	$\frac{R_{neck}}{R_{initial}}$
($147^{\circ}C$; sphere diameters 240 and 240 microns; initial sphere diameter readings 248 and 248)		
2:05	20	0.0806
4:00	30.5	.123
6:00	41	.165
9:30	51.5	.208
16:30	68.5	.276
27:00	90.5	.365
35:00	105	.433
48:20	126.5	.510
148:00	222.5	.895
($152^{\circ}C$; sphere diameters 233 and 234 microns; initial sphere diameter readings 241 and 242)		
1:20	33	.137
3:00	45.5	.188
6:30	73	.311
9:40	87	.360
15:10	108	.447
22:50	136	.563
44:30	194.5	.805
72:00	233	.965

Table C.5. Time, neck diameter measurements, and radius ratio of $As_{1/4}Se_3$

Time (minutes:seconds)	$2R_{neck}$	$\frac{R_{neck}}{R_{initial}}$
(95°C; sphere diameters 203 and 203 microns; initial sphere diameter readings 210 and 210)		
1:00	43	.205
2:00	50	.238
5:10	66	.314
8:50	71.5	.341
14:30	80	.381
32:00	118.5	.564
(96°C; sphere diameters 176 and 177 microns; initial sphere diameter readings 182 and 183)		
0:15	35.5	.195
1:00	40	.241
2:30	51.5	.282
5:30	60.5	.332
9:50	68.5	.375
16:10	83.0	.455
22:30	94.5	.518
33:00	112.0	.614

Table C.6. Time, neck diameter measurements, and radius ratio of $As_3S_{1/2}Se_{5/2}$

Time (minutes:seconds)	$2R_{neck}$	$\frac{R_{neck}}{R_{initial}}$
(236°C; sphere diameters 207 and 207 microns; initial sphere diameter readings 214 and 214; volatilization observed)		
1:45	30	.140
4:15	37	.172
14:00	48.5	.226
29:30	59	.274
67:00	73.5	.342
138:00	81	.377
203:00	84	.392
265:00	85	.397
378:00	89	.415
(225°C; sphere diameters 226 and 228 microns; initial sphere diameter readings 234 and 236; volatilization observed)		
6:15	37	.157
11:15	40	.170
19:00	45.5	.193
32:00	51.5	.219
45:00	58.0	.247
87:00	82	.349
156:00	91.5	.389

Table C.7. Time, neck diameter measurements, and radius ratio of $As_2S_{1/2}Se_{5/2}$

Time (minutes:seconds)	$2R_{neck}$	$\frac{R_{neck}}{R_{initial}}$
(234°C; sphere diameters 198 and 198 microns; initial sphere diameter readings 205 and 205)		
2:00	34.5	.168
5:00	42.5	.207
10:30	46.5	.227
17:30	52.5	.256
31:30	66.5	.324
47:00	73	.356
75:00	78	.380
97:00	87	.424
177:30	102	.498
433:00	134	.654
(228°C; sphere diameters 218 and 218 microns; initial sphere diameter readings 226 and 226)		
6:20	29.5	.131
12:30	36	.159
19:15	38	.168
34:00	44.5	.197
62:00	47	.208
120:00	52	.230
294:00	67	.296
550:00	91	.403

Table C.8. Time, neck diameter measurements, and radius ratio of $As_{5/4}S_{1/2}Se_{5/2}$

Time (minutes:seconds)	$2R_{neck}$	$\frac{R_{neck}}{R_{initial}}$
(211°C; sphere diameters 225 and 225 microns; initial sphere diameter readings 233 and 233)		
0:35	54	.232
1:15	71	.305
1:55	86	.369
2:35	99	.425
3:30	110	.472
5:00	125.5	.539
9:30	167	.717
(208°C; sphere diameters 193 and 194 microns; initial sphere diameter readings 200 and 201)		
0:35	37	.185
1:20	47	.235
2:35	63	.315
3:35	74	.370
4:35	85	.425
6:45	106	.530
7:40	113	.565
17:45	174	.870
(221°C; sphere diameters 218 and 218 microns; initial sphere diameter readings 226 and 226)		
0:45	62.5	.277
2:00	106.0	.470
3:00	131.0	.580
3:40	154.0	.681
4:40	177.0	.783
5:30	195.0	.863
6:15	207.0	.916
7:25	224.5	.991
9:00	242	1.071
13:15	271	1.199

Table C.9. Time, neck diameter measurements, and radius ratio of $As_{3/4}S_{1/2}Se_{5/2}$

Time (minutes:seconds)	$2R_{neck}$	$\frac{R_{neck}}{R_{initial}}$
(150°C; sphere diameters 272 and 272 microns; initial sphere diameter readings 282 and 282)		
3:00	42.5	.151
7:05	65	.230
13:45	88	.312
25:45	119	.422
36:15	141	.500
50:00	172	.610
65:00	198.5	.704
96:15	243.5	.857
119:30	266.5	.938
(164°C; sphere diameters 252 and 253 microns; initial sphere diameter readings 261 and 263)		
0:30	39	.149
1:20	55	.210
2:35	77	.294
3:35	96	.366
4:50	119	.454
6:10	142	.542
7:40	169.5	.647
9:45	200.0	.763
12:20	231.5	.884
19:15	274	1.046

Table C.10. Time, neck diameter measurements, and radius ratio of $As_{1/4}S_{1/2}Se_{5/2}$

Time (minutes:seconds)	$2R_{neck}$	$\frac{R_{neck}}{R_{initial}}$
(109°C; sphere diameters 214 and 213 microns; initial sphere diameter readings 222 and 221)		
0:30	59	.266
1:00	70	.315
2:10	85	.383
3:10	95	.428
4:10	104.5	.471
5:50	117.0	.527
8:30	139.5	.628
10:15	149.0	.671
(96°C; sphere diameters 228 and 228 microns; initial sphere diameter readings 236 and 236)		
3:30	36	.153
7:15	41	.174
9:00	44	.186
15:30	52	.220
24:00	59	.250
35:00	64	.271
54:00	79	.335
78:15	95.5	.405
97:00	117	.496
(103°C; sphere diameters 174 and 174 microns; initial sphere diameter readings 180 and 180)		
1:30	47	.261
3:00	53.5	.297
5:00	61	.339
7:00	69	.383
9:00	75.5	.419
11:00	83.5	.464
13:00	88.5	.492
19:40	107	.594
28:00	130	.722
39:30	152	.844

Table C.11. Time, neck diameter measurements, and radius ratio of As_3SSe_2

Time (minutes:seconds)	$2R_{neck}$	$\frac{R_{neck}}{R_{initial}}$
(225°C; sphere diameters 215 and 215 microns; initial sphere diameter readings 223 and 223; large volatilization losses)		
0:35	38	.171
4:30	44.5	.200
10:15	50.0	.224
33:00	47.5	.214
60:00	38.5	.173
(219°C; sphere diameters 200 and 201 microns; initial sphere diameter readings 207 and 208; large volatilization losses)		
8:00	25.5	.121
19:00	25.0	.121
36:00	26.0	.125

Table C.12. Time, neck diameter measurements, and radius ratio of As_2SSe_2

Time (minutes:seconds)	$2R_{neck}$	$\frac{R_{neck}}{R_{initial}}$
(241°C; sphere diameters 237 and 238 microns; initial sphere diameter readings 245 and 246; volatilization observed)		
13:00	47	.191
22:30	54	.220
36:10	61	.248
48:40	65	.264
150:00	94	.382
195:00	102.5	.417
263:00	116	.472
(246°C; sphere diameters 234 and 234 microns; initial sphere diameter readings 242 and 242; volatilization observed)		
5:00	39.5	.163
13:45	54.0	.223
25:40	67.5	.279
47:00	82.0	.339
174:00	121.0	.501

Table C.13. Time, neck diameter measurements, length measurements, radius ratio, and length ratio of $As_{5/4}SSe_2$

Time (minutes:seconds)	$2R_{neck}$	$\frac{R_{neck}}{R_{initial}}$
(202°C; sphere diameters 260 and 261 microns; initial sphere diameter readings 269 and 270; initial length measurement 541)		
4:00	37.5	0.139
5:45	47	0.174
8:45	59	0.219
15:45	84	.312
21:30	107	.397
28:45	133	.494
37:30	163.5	.607
44:20	187.5	.696
60:00	227.5	.844
73:40	256.5	.952
91:20	286.5	1.063
115:10	310.0	1.150
135:00	318.0	1.180
	Length	$\frac{Length}{Length_{initial}}$
4:45	539.5	0.995
6:30	537.5	0.992
9:30	535.5	0.988
16:20	533	0.984
22:15	531	0.979
29:40	525.5	0.969
38:10	514.0	0.948
45:00	510.0	0.940
60:00	489	0.902
74:45	464	0.858
92:45	438	0.810
116:20	406	0.751
136:15	392.5	0.725

Table C.13. (Continued)

Time (minutes:seconds)	$2R_{neck}$	$\frac{R_{neck}}{R_{initial}}$
($199^{\circ}C$; sphere diameters 244 and 244 microns; initial sphere diameter readings 253 and 253)		
8:45	51	.202
11:15	58	.229
15:20	66.5	.263
20:05	76.0	.300
30:15	104.0	.411
38:00	123.5	.488
67:45	192.5	.761
84:20	221.5	.875
92:30	232.5	.918

Table C.14. Time, neck diameter measurements, radius ratio of $As_3/4SSe_2$

Time (minutes:seconds)	$2R_{neck}$	$\frac{R_{neck}}{R_{initial}}$
(158°C; sphere diameters 248 and 248 microns; initial sphere diameter readings 257 and 257)		
3:20	58	.225
5:10	71.5	.278
7:40	84	.327
12:00	106	.412
14:00	123	.479
18:30	150	.584
21:30	176	.685
26:00	200	.778
36:00	238.5	.928
(160°C; sphere diameters 233 and 234 microns; initial sphere diameter readings 241 and 243)		
1:20	35	.145
2:20	48.5	.200
4:05	71	.293
5:40	85	.351
7:25	97	.401
9:00	107	.442
14:00	139	.574
18:30	158.5	.655
24:20	191.0	.789
31:40	219.5	.907
42:00	254.0	1.050

Table C.15. Time, neck diameter measurements, and radius ratio of $As_{1/4}SSe_2$

Time (minutes:seconds)	$2R_{neck}$	$\frac{R_{neck}}{R_{initial}}$
($112^{\circ}C$; sphere diameters 224 and 225 microns; initial sphere diameter readings 232 and 233)		
0:50	53.5	.231
1:30	65.5	.282
2:30	81	.348
3:45	100	.430
4:45	107.5	.462
7:20	132.5	.570
11:00	160	.688
17:15	206.5	.884
($103^{\circ}C$; sphere diameters 210 and 211 microns; initial sphere diameter readings 217 and 218)		
2:15	42	.193
3:40	47.5	.218
5:15	56.5	.260
6:45	64.5	.297
9:15	73	.336
12:40	85	.391
15:10	93	.428
20:50	107.5	.494
26:00	125	.575
36:45	153	.703
51:20	183.5	.844
73:15	213.5	.982
93:00	229	1.053

Table C.16. Time, neck diameter measurements, radius ratio of $As_3S_{3/2}Se_{3/2}$

Time (minutes:seconds)	$2R_{neck}$	$\frac{R_{neck}}{R_{initial}}$
($225^{\circ}C$; sphere diameters 196 and 198 microns; initial sphere diameter readings 203 and 205; large volatilization losses)		
2:15	23.5	.115
27:00	18.5	.091
149:00	20.5	.101
($235^{\circ}C$; sphere diameters 193 and 193 microns; initial sphere diameter readings 200 and 200; large volatilization losses)		
1:20	30.5	.152
8:00	34.0	.170
23:00	34.0	.170

Table C.17. Time, neck diameter measurements, radius ratio of $As_2S_{3/2}Se_{3/2}$

Time (minutes:seconds)	$2R_{neck}$	$\frac{R_{neck}}{R_{initial}}$
(258°C; sphere diameters 257 and 258 microns; initial sphere diameter readings 266 and 267; volatilization losses)		
0:30	40.5	.151
1:35	52	.195
3:00	65	.243
5:00	73.5	.275
7:15	79.5	.298
10:30	87	.326
13:30	90.5	.339
20:00	96	.360
32:00	99.5	.373
55:00	101.0	.378
105:00	117.0	.441
(254°C; sphere diameters 267 and 267 microns; Initial sphere diameter readings 277 and 277; volatilization losses)		
2:45	37	.134
4:30	45	.164
7:00	53	.191
15:00	65.5	.236
33:15	80.0	.289
46:30	84.0	.303

Table C.18. Time, neck diameter measurements, length measurements, radius ratio, and length ratio of $As_{5/4}S_{3/2}Se_{3/2}$

Time (minutes:seconds)	$2R_{neck}$	$\frac{R_{neck}}{R_{initial}}$
(198°C; sphere diameters 336 and 335 microns; initial sphere diameter readings 244 and 243; initial length 487.5)		
3:00	53.5	.220
5:45	73.5	.302
7:40	88	.361
10:15	108	.444
12:30	133.5	.548
14:45	151.0	.620
17:35	172.0	.706
20:10	190.5	.782
27:50	227.5	.934
36:45	261.0	1.072
50:00	286	1.174
60:30	296.5	1.215
	Length	$\frac{Length}{Length_{initial}}$
3:00	485.5	.996
6:45	485	.994
8:30	479	.983
11:15	474	.972
13:50	468.4	.962
15:45	462	.946
18:45	457	.936
21:25	438	.900
29:20	411.5	.842
37:40	379	.777
51:45	358.5	.734
61:20	343	.703

Table C.18. (Continued)

Time (minutes:seconds)	$2R_{neck}$	$\frac{R_{neck}}{R_{initial}}$
(194°C; sphere diameters 194 and 198 microns; initial sphere diameter readings 200.5 and 204.5; initial length 402)		
5:00	51.5	.255
8:00	68	.337
11:00	79.5	.394
13.50	92.5	.458
17:30	110	.545
19:45	119	.589
29:00	147	.728
48:40	191.5	.948
123:00	250	1.238
	Length	$\frac{Length}{Length_{initial}}$
6:15	401.5	.999
9:10	398.0	.990
12:30	392.0	.975
15:15	391.0	.973
18:40	384.0	.955
20:50	383.5	.954
29:45	368.5	.917
49:50	339.0	.843
124:00	285.0	.709

Table C.19. Time, neck diameter measurements, length measurements, radius ratio, length ratio of $As_{3/4}S_{3/2}Se_{3/2}$

Time (minutes:seconds)	$2R_{neck}$	$\frac{R_{neck}}{R_{initial}}$
(155°C; sphere diameters 251 and 252 microns; initial sphere diameter readings 259 and 260)		
1:40	52.5	.203
2:40	64	.247
3:45	74	.286
5:10	83.5	.322
7:00	98.5	.380
8:30	111.0	.429
10:00	124.0	.479
16:15	178.0	.687
21:00	214.5	.828
24:30	233.5	.902
30:30	255.5	.986
(157°C; sphere diameters 308 and 309 microns; initial sphere diameter readings 319 and 320; initial length 638)		
0:45	55	.172
1:25	67	.210
2:00	76	.238
3:25	92.5	.290
4:20	105.5	.331
5:20	118.0	.370
6:10	129.0	.404
7:35	146.0	.458
8:35	155.5	.487
14:45	230	.721
19:10	261.5	.820
24:30	298	.934
33:30	319.5	1.002
	Length	$\frac{Length}{Length_{initial}}$
33:30	533.5	.836

Table C.20. Time, neck diameter measurements, radius ratio of $As_{1/4}S_{3/2}Se_{3/2}$

Time (minutes:seconds)	$2R_{neck}$	$\frac{R_{neck}}{R_{initial}}$
($101^{\circ}C$; sphere diameters 167 and 167 microns; initial sphere diameter readings 173 and 173)		
1:35	40.5	.286
3:00	57.0	.329
4:30	65.0	.376
6:30	75.0	.434
9:30	86.0	.497
12:30	96.5	.558
18:20	113.5	.656
23:30	126.0	.728
33:00	144.5	.835
38:45	156.5	.905
46:15	165.5	.957
61:15	180.0	1.040
($118^{\circ}C$; sphere diameters 189 and 188 microns; initial sphere diameter readings 196 and 195)		
0:50	67	.333
2:00	87	.432
2:50	98	.486
3:35	111	.551
4:30	121.5	.603
5:30	136	.675
6:30	148.5	.737
7:30	161	.799
8:15	169	.839
10:30	188	.933
13:20	208	1.032
19:30	231.5	1.149
24:00	242.5	1.203

Table C.20. (Continued)

Time (minutes:seconds)	$2R_{neck}$	$\frac{R_{neck}}{R_{initial}}$
($119^{\circ}C$; sphere diameters 190 and 191 microns; initial sphere diameter readings 197 and 198)		
0:30	56	.284
1:15	75	.380
1:50	92	.466
2:20	102	.516
3:30	128.5	.651
4:10	142.0	.719
4:50	153	.775
6:10	171	.866
6:50	181	.916
13:35	223	1.129

Table C.21. Time, neck diameter measurements, radius ratio of As_3S_2Se

Time (minutes:seconds)	$2R_{neck}$	$\frac{R_{neck}}{R_{initial}}$
($234^{\circ}C$; sphere diameters 194 and 196 microns; initial sphere diameter readings 201 and 203; large volatilization losses)		
0:45	24.5	.121
7:30	28.0	.139
28:00	28.0	.139
55:30	35.0	.173

Table C.22. Time, neck diameter measurements, radius ratio of As_2S_2Se

Time (minutes:seconds)	$2R_{neck}$	$\frac{R_{neck}}{R_{initial}}$
(273°C; sphere diameters 187 and 187 microns; initial sphere diameter readings 193 and 193; volatilization losses)		
3:45	43	.223
5:15	52	.269
9:30	72.5	.375
12:45	78	.404
24:00	98	.508
(286°C; sphere diameters 180 and 181 microns; initial sphere diameter readings 186 and 187; volatilization losses)		
1:05	37	.199
2:00	50.5	.271
3:00	59.5	.320
5:00	70.0	.376
7:30	76.0	.409
13:30	97.0	.521
(280°C; sphere diameters 178 and 179 microns; initial sphere diameter readings 184 and 185; volatilization losses)		
0:30	24.5	.132
1:30	37.5	.203
2:20	42.0	.227
3:20	48.0	.259
5:00	54.0	.292
6:20	62.0	.335
8:00	62.0	.335
11:35	64.0	.346
18:45	77.0	.416
23:50	80.0	.432
30:45	92.5	.500

Table C.23. Time, neck diameter measurements, radius ratio of $As_{5/4}S_2Se$

Time (minutes:seconds)	$2R_{neck}$	$\frac{R_{neck}}{R_{initial}}$
(213°C; sphere diameters 178 and 178 microns; initial sphere diameter readings 184 and 184)		
0:45	62	.294
1:30	94	.446
2:50	143	.678
4:15	177	.840
6:05	204.5	.970
7:40	221.0	1.050
9:45	238.5	1.132
11:25	249.5	1.183
13:10	265.5	1.260
(198°C; sphere diameters 206 and 207 microns; initial sphere diameter readings 213 and 214)		
2:00	34	.159
4:40	55	.258
8:30	72	.337
14:00	99	.464
20:00	146.5	.686
24:35	178.5	.836
28:40	197.0	.923
34:00	223.5	1.047
41:00	247.0	1.157
47:20	261.0	1.222

Table C.24. Time, neck diameter measurements, length measurements, radius ratio, length ratio of $As_{3/4}S_2Se$

Time (minutes:seconds)	$2R_{neck}$	$\frac{R_{neck}}{R_{initial}}$
(134°C; sphere diameters 186 and 187 microns; initial sphere diameter readings 192 and 193; initial length 384.5)		
8:00	36	.187
14:15	44	.229
31:00	60.5	.314
61:00	70.5	.366
75:30	80.5	.420
90:00	91.0	.473
149:00	117.0	.608
	Length	$\frac{Length}{Length_{initial}}$
6:20	384.5	1.000
15:15	383.5	.997
32:00	381	.991
61:40	378.5	.984
76:40	377	.980
90:30	376	.978
149:00	370	.962
(152°C; sphere diameters 193 and 193 microns; initial sphere diameter readings 200 and 200)		
1:00	43	.215
2:35	48	.240
5:00	55	.278
9:00	64	.320
12:30	70.5	.353
20:30	83	.415
27:30	92.5	.462
37:00	109.0	.545
53:15	138.0	.690
60:00	148.0	.740

Table C.24. (Continued)

Time (minutes:seconds)	$2R_{neck}$	$\frac{R_{neck}}{R_{initial}}$
(156°C; sphere diameters 174 and 174 microns; initial sphere diameter readings 180 and 180)		
0:30	49.5	.275
1:30	67.5	.375
2:00	78	.433
3:00	92	.511
4:05	116.5	.647
7:15	171.5	.953
12:30	214.0	1.189

Table C.25. Time, neck diameter measurements, radius ratio of $As_{1/4}S_2Se$

Time (minutes:seconds)	$2R_{neck}$	$\frac{R_{neck}}{R_{initial}}$
($116^{\circ}C$; sphere diameters 169 and 169 microns; initial sphere diameter readings 175 and 175)		
0:30	37	.211
1:15	47.5	.271
2:10	56	.320
3:30	64.5	.369
4:50	71.0	.406
6:15	84.5	.483
7:30	89.0	.508
9:05	98.0	.560
11:20	113.5	.649
14:35	128.0	.731
18:00	148.5	.849
25:15	171.5	.980
33:45	191.5	1.094
44:45	207.0	1.183
($111^{\circ}C$; sphere diameters 175 and 175 microns; initial sphere diameter readings 181 and 181)		
0:35	42	.233
2:00	51.5	.286
3:30	57.5	.319
5:00	65	.361
7:00	69.5	.386
8:30	71.5	.397
12:30	77.0	.428
17:30	87.5	.486
22:10	94.0	.522
29:30	106	.589
37:15	117	.649

Table C.26. Time, neck diameter measurements, radius ratio of $As_3S_{5/2}Se_{1/2}$

Time (minutes:seconds)	$2R_{neck}$	$\frac{R_{neck}}{R_{initial}}$
(211°C; sphere diameters 183 and 183 microns; initial sphere diameter readings 189 and 189; large volatilization losses)		
1:15	23	.121
9:45	24	.127
30:00	25	.132
176:00	33	.175

Table C.27. Time, neck diameter measurements, length measurements, radius ratio, and length ratio of $As_2S_{5/2}Se_{1/2}$

Time (minutes:seconds)	$2R_{neck}$	$\frac{R_{neck}}{R_{initial}}$
(280°C; sphere diameters 174 and 174 microns; initial sphere diameter readings 180 and 180; initial length 360)		
1:45	32.5	.181
4:00	48	.267
6:30	56.5	.314
9:40	71	.394
11:45	76	.422
13:50	81	.450
15:50	88	.489
24:00	108.5	.603
31:10	126.5	.703
49:00	156.0	.867
65:10	178.0	.989
83:00	193.5	1.075
98:15	200.5	1.114
263:00	222.0	1.233

Table C.27. (Continued)

Time (minutes:seconds)	Length	$\frac{\text{Length}}{\text{Length}_{initial}}$
3:00	358.0	.994
5:40	357.0	.990
8:45	354.5	.985
11:00	354.5	.985
12:45	352.5	.980
14:45	352.0	.978
22:30	345.5	.960
29:40	339.0	.942
37:00	333.0	.925
50:30	322.5	.896
62:45	309.0	.858
81:00	290.5	.807
96:15	279.0	.775
264.00	246.0	.685
	$2R_{neck}$	$\frac{R_{neck}}{R_{initial}}$
($275^{\circ}C$; sphere diameters 174 and 176 microns; initial sphere diameter readings 179 and 181)		
4:00	38.0	.212
8:00	47.5	.265
14:00	60.0	.335
20:30	70.0	.388
31:00	84.5	.470
46:00	100.0	.555
72:00	130.0	.722
98:30	154.5	.858
165:00	189.5	1.052
200:00	200.0	1.112
258:00	207.0	1.150
300:00	208.5	1.158

Table C.28. Time, neck diameter measurements, length measurements, radius ratio, and length ratio of $As_{5/4}S_{5/2}Se_{1/2}$

Time (minutes:seconds)	$2R_{neck}$	$\frac{R_{neck}}{R_{initial}}$
(200°C; sphere diameters 188 and 189 microns; initial sphere diameter readings 194 and 195; initial length 390)		
12:00	41	.211
14:35	46.5	.239
17:00	52.2	.270
19:20	54.5	.280
24:35	61	.350
29:30	68	.350
38:30	80	.411
49:45	101	.519
70:10	124	.638
87:00	142.5	.733
105:30	157.0	.807
132:15	169.5	.871
203:00	190.5	.979
440:00	201.0	1.033
1250:00	208.0	1.069
	Length	$\frac{Length}{Length_{initial}}$
13:00	385	.988
15:35	384.5	.987
18:05	384	.986
21:15	383.5	.985
27:15	383	.983
31:30	381	.979
40:00	379.5	.974
52:00	377	.968
69:10	366	.940
86:00	359	.922
104:15	356.5	.915
130:45	345	.887
201:00	330.5	.848
442:00	323.5	.830
1250:00	314	.800

Table C.28. (Continued)

Time (minutes:seconds)	$2R_{neck}$	$\frac{R_{neck}}{R_{initial}}$
(202°C; sphere diameters 174 and 175 microns; initial sphere diameter readings 180 and 181; initial length 361)		
2:40	35	.193
5:05	44	.243
6:40	50	.276
8:50	59	.326
10:30	63	.348
12:05	67	.370
13:55	70	.387
17:25	77.5	.428
21:10	89	.492
23:30	90	.497
27:30	101.5	.561
29:45	108.0	.599
35:00	119.0	.657
41:30	129.5	.715
46:35	140.0	.774
53:45	150.0	.829
60:00	157.0	.867
72:00	170.5	.942
79:30	176.0	.972
173:00	209.5	1.157
	Length	$\frac{Length}{Length_{initial}}$
3:45	360	.997
5:55	357.5	.990
7:30	359	.994
9:30	359	.994
11:15	356.5	.988
12:55	356.5	.988
16:20	355	.983
20:15	355	.983
22:05	353	.978

Table C.28. (Continued)

Time (minutes:seconds)	Length	$\frac{\text{Length}}{\text{Length}_{\text{initial}}}$
25:00	351	.972
28:45	347.5	.963
31:05	346.5	.960
36:15	344.5	.954
42:30	339.0	.940
47:50	334.0	.925
54:45	329.0	.910
61:05	323.5	.895
73:15	316.0	.875
80:40	308.5	.853
175:00	276.0	.763

Table C.29. Time, neck diameter measurements, radius ratio of $As_{3/4}S_{5/2}Se_{1/2}$

Time (minutes:seconds)	$2R_{neck}$	$\frac{R_{neck}}{R_{initial}}$
(179°C; sphere diameters 196 and 197 microns; initial sphere diameter readings 203 and 204)		
1:10	51	.245
3:45	83.5	.401
6:10	99	.476
8:40	114.5	.551
11:25	131.5	.632
14:05	150.5	.724
16:45	165	.793
19:05	178	.856
21:40	191	.918
24:05	204	.981
26:30	213	1.024
35:30	236	1.135
(174°C; sphere diameters 180 and 184 microns; initial sphere diameter readings 186 and 190)		
3:00	57.5	.306
5:25	70	.372
7:40	84	.447
10:10	102.5	.545
13:15	126	.670
15:15	141	.750
17:50	157.5	.838
20:20	172	.915
23:00	185	.984
25:50	197.5	1.051
28:50	206.5	1.099
31:15	214	1.138

Table C.30. Time, neck diameter measurements, length measurements, radius ratio, and length ratio of $As_{1/4}S_{5/2}Se_{1/2}$

Time (minutes:seconds)	$2R_{neck}$	$\frac{R_{neck}}{R_{initial}}$
(111°C; sphere diameters 170 and 170.5 microns; initial sphere diameter readings 176 and 175.5; initial length 342.5)		
0:40	53	.302
2:50	64	.365
4:50	70	.399
6:45	74	.422
8:40	78	.444
10:40	79	.450
15:40	87.5	.499
22:30	90.5	.516
37:45	98.0	.558
51:45	100	.570
75:00	107.5	.613
88:30	108.0	.615
231:00	149.0	.849
	Length	$\frac{Length}{Length_{initial}}$
1:45	340	.993
3:50	340	.993
6:00	337.5	.986
7:40	335.5	.980
9:40	332.5	.971
14:45	331.0	.967
21:30	328.5	.959
35:30	329.0	.961
50:30	327.5	.956
73:10	325.0	.949
91:00	323.0	.943
227:00	304	.890

Table C.30. (Continued)

Time (minutes:seconds)	$2R_{neck}$	$\frac{R_{neck}}{R_{initial}}$
(110°C; sphere diameters 187 and 187 microns; initial sphere diameter readings 193 and 193)		
0:50	43	.223
1:50	45	.233
3:30	47.5	.246
6:20	53.0	.275
10:15	58	.301
19:20	64	.332
28:30	68	.352
42:15	72	.373
129:00	86	.446
245:00	105	.544
302:00	112	.580
(116°C; sphere diameters 179 and 179 microns; initial sphere diameter readings 185 and 185)		
0:20	64	.348
2:35	84.5	.459
4:45	92	.500
8:15	102.5	.557
12:50	117.5	.639
21:10	138	.750
31:00	158	.859
45:00	168	.913
64:00	178	.967

Table C.31. Time, neck diameter measurements, radius ratio of As_3S_3

Time (minutes:seconds)	$2R_{neck}$	$\frac{R_{neck}}{R_{initial}}$
(195°C; sphere diameters 251 and 252 microns; initial sphere diameter readings 259 and 260; large volatilization losses)		
20:00	20	.077
136:30	23	.088
187:30	40.5	.156
236:00	41.5	.160
307:30	34	.131
(166°C; sphere diameters 222 and 224 microns; initial sphere diameter readings 230 and 234; large volatilization losses		
25:00	35.5	.153
69:00	48.0	.207
269:00	54.0	.233
800:00	55.5	.239

Table C.32. Time, neck diameter measurements, radius ratio of As_2S_3

Time (minutes:seconds)	$2R_{neck}$	$\frac{R_{neck}}{R_{initial}}$
(304°C; sphere diameters 232 and 232 microns; initial sphere diameter readings 240 and 240)		
3:30	63	.263
5:30	77	.321
7:00	86	.358
9:30	93.5	.390
12:30	110.0	.458
(312°C; sphere diameters 222 and 228 microns; initial sphere diameter readings 229 and 235)		
0:20	52	.224
0:55	75	.323
1:30	95.5	.412
2:10	118.0	.509
3:00	130.5	.562
3:35	144.0	.620
4:30	155.5	.670
5:50	171.0	.737
8:00	191.0	.823
12:00	221.5	.955
23:15	256.0	1.103

Table C.33. Time, neck diameter measurements, length measurements, radius ratio, and length ratio of $As_{5/2}S_3$

Time (minutes:seconds)	$2R_{neck}$	$\frac{R_{neck}}{R_{initial}}$
(205°C; sphere diameters 162.5 and 163.5 microns; initial sphere diameter readings 168 and 169; initial length 337)		
28:45	40	.237
64:00	67	.398
102:00	91.5	.543
138:00	111.5	.661
166:00	122.5	.727
567:00	169.0	1.003
	Length	$\frac{Length}{Length_{initial}}$
29:30	332	0.985
65:00	328	0.975
103:00	323	0.961
140:00	315.5	0.936
167:00	313	0.929
567:00	283.0	0.840
(208°C; sphere diameters 187 and 185 microns; initial sphere diameter readings 193 and 191; initial length 384)		
20:00	42	.219
23:30	45	.234
28:00	53	.276
31:10	58.5	.305
42:20	69	.359
56:00	77	.401
71:00	87.5	.456

Table C.33. (Continued)

Time (minutes:seconds)	$2R_{neck}$	$\frac{R_{neck}}{R_{initial}}$
142:00	152.0	.792
176:00	174.0	.906
206:00	185.0	.964
241:00	199.0	1.036
276:00	204.5	1.065
425:00	220.0	1.146
454:00	221.0	1.151
499:00	221.5	1.154
	Length	$\frac{Length}{Length_{initial}}$
21:00	380	.990
24:00	378.5	.986
29:00	378	.984
32:00	378	.984
43:00	377.5	.983
57:00	374.0	.975
72:15	368	.958
143:00	349	.910
177:00	336	.875
207:00	327	.852
242:00	316	.823
277:00	309	.804
426:00	286	.745
455:15	282.5	.736
498:00	277.5	.722

Table C.34. Time, neck diameter measurements, radius ratio of $As_{3/4}S_3$

Time (minutes:seconds)	$2R_{neck}$	$\frac{R_{neck}}{R_{initial}}$
(148°C; sphere diameters 163.5 and 161.5 microns; initial sphere diameter readings 169 and 167)		
1:00	30	.179
2:00	34.5	.205
5:10	43	.256
9:15	48.5	.289
15:00	54.5	.324
22:00	60	.357
32:00	64	.381
44:00	68	.405
60:00	75	.446
(152°C; sphere diameters 169 and 169 microns; initial sphere diameter readings 175 and 175)		
0:30	32.5	.186
1:35	38.0	.217
2:45	44.5	.254
4:00	50.0	.286
5:30	56.5	.323
6:35	59.0	.337
7:45	62.0	.354
11:00	65.0	.371
17:30	71.0	.406
24:00	80.0	.457
34:30	85.0	.486
54:00	102.0	.583

Table C.35. Time, neck diameter measurements, length measurements, radius ratio, and length ratio of As1/48

Time (minutes:seconds)	$2R_{neck}$	$\frac{R_{neck}}{R_{initial}}$
(129°C; sphere diameters 215 and 218 microns; initial sphere diameter readings 222 and 225)		
1:00	82	.307
2:00	93.5	.350
2:40	101.0	.378
3:30	106	.397
4:20	110	.412
5:20	121	.453
7:05	128	.479
9:30	133	.498
11:15	141.5	.530
15:05	156	.584
20:50	171	.640
(116°C; sphere diameters 223 and 218 microns; initial sphere diameter readings 231 and 226; initial length 465)		
0:30	69	.302
1:45	80	.350
3:30	82.5	.361
5:15	91.5	.400
7:45	104.0	.455
10:00	115.0	.503
12:15	121.0	.529
14:10	127.0	.556
16:40	136.0	.595
20:50	152.0	.665
28:00	169.0	.740
35:30	180.5	.790
47:15	193.0	.845

Table C.35. (Continued)

Time (minutes:seconds)	Length	$\frac{\text{Length}}{\text{Length}_{\text{initial}}}$
4:30	458	.985
7:00	454	.976
9:05	452	.972
11:15	451	970
13:15	448	.965
15:15	446	.961
19:45	440.5	.948
22:25	435	.936
29:30	430	.925
45:30	421	.905

ACKNOWLEDGEMENTS

The author wishes to express his gratitude to Messrs. D. Van Zuuk and R. C. Prior for their help with the heater control, to Mr. D. H. Erbeck for use of his computer program, to Mr. W. R. McMahon for his encouragement during the course of this research, and especially to Dr. D. R. Wilder for his guidance in the course of this work.